Journal of Energy Storage 49 (2022) 103743

Contents lists available at ScienceDirect

Journal of Energy Storage

journal homepage: www.elsevier.com/locate/est

Research papers

SimSES: A holistic simulation framework for modeling and analyzing stationary energy storage systems

Marc Möller [a,*], Daniel Kucevic [a], Nils Collath [a], Anupam Parlikar [a], Petra Dotzauer [b], Benedikt Tepe [a], Stefan Englberger [a], Andreas Jossen [a], Holger Hesse [a]

[a] Institute for Electrical Energy Storage Technology, Technical University of Munich (TUM), Arcisstr. 21, 80333 Munich, Germany
[b] Bavarian Center for Applied Energy Research (ZAE Bayern), Department of Energy Storage, Walther-Meiner-Str. 6, 85748 Garching, Germany

ARTICLE INFO

Keywords:
Energy storage system simulation
Lithium-ion battery
Redox flow battery
Hydrogen technology
Storage system design
Stationary application

ABSTRACT

The increasing feed-in of intermittent renewable energy sources into the electricity grids worldwide is currently leading to technical challenges. Stationary energy storage systems provide a cost-effective and efficient solution in order to facilitate the growing penetration of renewable energy sources. Major technical and economical challenges for energy storage systems are related to lifetime, efficiency, and monetary returns. Holistic simulation tools are needed in order to address these challenges before investing in energy storage systems. One of these tools is SimSES, a holistic simulation framework specialized in evaluating energy storage technologies technically and economically. With a modular approach, SimSES covers various topologies, system components, and storage technologies embedded in an energy storage application. This contribution shows the capabilities and benefits of SimSES by providing in-depth knowledge of the implementations and models. Selected functionalities are demonstrated, with two use cases showing the easy-to-use simulation framework while providing detailed technical analysis for expert users. Hybrid energy storage systems consisting of lithium-ion and redox-flow batteries are investigated in a peak shaving application, while various system topologies are analyzed in a frequency containment reserve application. The results for the peak shaving case study show a benefit in favor of the hybrid system in terms of overall cost and degradation behavior in applications that have a comparatively low energy throughput during lifetime. In terms of system topology, a cascaded converter approach shows significant improvements in efficiency for the frequency containment reserve application.

1. Introduction

In former decades, the worldwide energy transition was predominantly driven by introducing more Renewable Energy Sources (RES) capacity to existing power networks, a process strongly supported by both globally declining cost for wind and solar power generation as well as through local legislation support, including subsidy schemes [1,2]. Following these early stage developments, the energy transition in various regions has now started to face new constraints and technical challenges, which demand other and often more site-specific solution approaches. Coupling of the power grid to both heating and electrified transport is certainly a key strategy to increase RES penetration on a global and nationwide level within the power system itself. At the same time, increasing the intermittence of supply that relies more on variable sources like solar and wind generation brings incorporation of grid-tied energy storage into discussion as a technically mature and potentially cost-competitive measure addressing volatility issues [3].

In order to categorize storage integration in power grids we may distinguish among Front-The-Meter (FTM) and Behind-the-Meter (BTM) applications [4]. FTM includes applications such as storage-assisted renewable energy time shift [5], wholesale energy arbitrage [6,7], and Frequency Containment Reserve (FCR) provision [8]. A more distributed and locally coordinated power supply is discussed in the context of BTM applications, e.g., Peak Shaving (PS) for industrial sites or at electric vehicle charging stations [9], or bill-saving at residential sites through Self-Consumption Increase (SCI) with local photovoltaic generation (residential battery storage) [10]. However, before taking a solid investment decision, it is crucial to analyze and optimize the technical parameters, storage dispatch control, as well as cost/revenue streams over the course of the entire project lifetime. Simulation and modeling tools in conjunction with sensitivity analyzes and optimization routines are commonly used to support these crucial steps in the planning and operational phase of grid-integrated storage projects.

* Corresponding author.
E-mail address: marc.moeller@tum.de (M. Möller).

https://doi.org/10.1016/j.est.2021.103743
Received 10 March 2021; Received in revised form 30 August 2021; Accepted 2 December 2021
Available online 24 February 2022

The Simulation Tool for Stationary Energy Storage Systems (**SimSES**) was developed to assist through the aforementioned tasks of storage system planning and operation. Through combining user-defined inputs with pre-parameterized component building blocks, as well as calculation methods and result analysis functions, a reserve is built for research, industry, and policy makers in equal measure to support deployment and enrollment of storage integration to the grid. The approach of **SimSES** is presented within this contribution.

In Section 2, comparable existing tools are reviewed and evaluated before the structure of **SimSES** is elaborated further in Section 3 as well as its detail models for storage technologies (Section 4) and its periphery (Section 5). Afterwards, in Section 6 two case studies are presented to show the capabilities of **SimSES** and concludes with a summary and outlook of further investigations in Section 7.

2. Literature review

Various authors have analyzed sizing and (economically) optimal operation of a specifically chosen storage system in a dedicated application setting, e.g., the usage of redox flow battery (RFB) for industrial PS applications [9] or the usage of lithium-ion battery (LIB) for SCI [11, 12]. Fewer studies exist comparing the suitability of different storage options for a given use case, e.g., refer to Toledo et al. [13] for a suitability comparison of different storage types for conducting residential self-consumption increase. Also, the profitability attainable across different applications was analyzed with a given technology to start off with, e.g., LIB in a wide range of application settings [14]. There is consensus that no uniform ideal candidate to meet all application-specific requirements exists within the storage technologies available to date [15]. In order to predict internal states of a storage system such as the State of Health (SOH) or the storage internal losses, it may become necessary to parameterize and simulate an adequately complex model of a storage system. Furthermore, simulations need to be fed with an operational concept that complies with the application constrains, and may deliver the compatibility of a given configuration as well as provide state predictions for the storage system. From an investor's perspective and ultimately for the most cost-effective integration of storage system to power grids with a high share of Variable Renewable Energy Sources (vRES), it is detrimental to conduct in-depth sensitivity and optimization studies relying on a full spectrum techno-economic model before subsequent tasks of project acquisition, realization, operation, and ultimately disposal are to be considered.

In the following, an overview of a selection of depicted tools for the techno-economic modeling of stationary storage in grid applications is provided. While Table 1 summarizes some of the main characteristics of these tools, it should be noted that this paper does not claim to provide a complete overview of all tools that may be relevant in the context matter.

GridLab-D,[1] developed and distributed via Pacific Northwest National Laboratory (*PNNL*), is a universal tool that allows modeling and analyzing multi-component power system networks. Its strength lies in the ability to simulate physical properties of various components through setting up and solving multiple differential equations, describing all sub-components in the modeling region. While the tool is certainly strong in modeling an entire micro-grid with its numerous grid states, it lacks detailed performance models for energy storage systems as well as application-specific parameterization and is therefore not applicable for detailed techno-economic analysis and optimization of storage project as it is focused in this work.

Other tools like **NAS Battery Simulator**,[2] **PNNL Flow Battery Calculator**,[3] and **H2FAST**,[4] are tools dedicated to specific storage types being sodium sulfur battery (NaS) redox flow, and electrolysis/hydrogen storage, respectively. These tools are developed for conducting rapid cost-revenue calculations for the specific technology of choice and offer limited user-specific input in terms of system parameterization and choice of application use case. Nevertheless, the aforementioned tools are confined to a dedicated storage system technology, rendering them less suitable for cross-technology comparisons. Furthermore, most tools of this kind are distributed as a proprietary code, matching only a dedicated commercial product well, and are not suitable for conducting sensitivity analyzes and adaption to envisioned new storage system control and operation.

More tailored simulations can be conducted using the tool **PerModAC** developed at htw Berlin [16]. Using this open-source software tool, performance and efficiency modeling of PV-coupled residential battery storage systems can be conducted. While the tool is extraordinarily strong in conducting battery storage product-specific performance and efficiency modeling, the model lacks the capabilities to analyze battery degradation. More importantly, the current version of this open-source tool is strictly confined to a specific residential BTM use case and cannot be used directly for cross-application assessments, as is desired for an investor's decision support.

Homer Pro and **Homer Grid** are more versatile modeling tools when it comes to comparing and optimizing the techno-economic performance of storage systems in (micro-)grids. The tools support various storage specific libraries and application-specific modeling capabilities, e.g., storage-supported renewable energy time shift in island grids as well as peak-shaving and solar-plus storage calculations in the current professional versions, and has been used in various scientific publications [17,18]. The software was developed by National Renewable Energy Laboratory (*NREL*), but the license for these tools are distributed solely via *Homerenergy* as a commercial product and cannot be extended/adapted according to the users' desire to address new application scenarios, specific personal needs, or local regulation frameworks. E.g., applications like the provision of frequency containment reserve and arbitrage marketing scenarios are not covered in the current version of the software tools.

Two other tools developed by *NREL* and Sandia National Laboratories (*SNL*) are worth looking at in more detail: **BLAST**[5] (Battery Lifetime Analysis and Simulation Tool) is a powerful software suite programmed using MATLAB® and it is distributed for both vehicle and stationary BTM applications. BLAST-BTM-Lite has powerful modeling capabilities for battery performance and lifetime calculations in stationary BTM applications and it includes both optimization and basic economic calculations. While it is highly recommended that this tool to be looked at closer by users interested in PV self-consumption and PS application, applications (only BTM) and storage systems to be analyzed (only conventional electro-chemical batteries) are clearly limited and confined. Furthermore, its original code structure lies hidden behind a graphical user interface and a proprietary executable file, making it unfeasible for the end-user to adapt parameters, e.g., sample time for peak shaving control.

The System Advisor Model[6] (**SAM**) tool builds up on a PV modeling framework originally set up by *SNL* and is now distributed via *NREL*. In its current version it allows coupling of battery storage with PV systems and incorporates financial models, e.g., for Power Purchase Agreement (PPA) calculations. More importantly, the user interface has been re-factored and is now distributed as an open-source software development kit for the Python programming language, allowing others to contribute with their individual extensions and developments. Nevertheless, on the technology side of its current version only batteries are supported and implemented (no other storage media).

[1] https://www.gridlabd.org/

[2] https://www.ngk-insulators.com/en/product/nas/simulator/

[3] https://github.com/PNNL-OE-Redox-Flow-Battery-Cost-Tool/PNNL-OE-Redox-Flow-Battery-Cost-Tool

[4] https://www.nrel.gov/hydrogen/h2fast.html

[5] https://www.nrel.gov/transportation/blast-btm-lite.html

[6] https://sam.nrel.gov/about-sam.html

Table 1
Overview of technical and economic modeling tools for energy storage in stationary applications.

Tool name	License type	Developer (primary)	Focus
GridLab-D	BSD open license	PNNL	Multi-domain state modeling for power distribution system simulation
NAS Battery Simulator	commercial	NGK-insulators	NGK product-tailored NaS battery simulation in peak shaving application
Flow Battery Calculator	open source	PNNL	Estimation tool of cost for redox flow batteries
H2FAST	open source (Excel sheet)	NREL	Economic assessment of hydrogen fuel stations
PerModAC	open source	htw	Performance and efficiency modeling of PV coupled residential battery storage systems
Homer Pro	commercial	Homerenergy (UL.com)	Residential/Microgrid modeling—multiple storage systems, multiple application scenarios
BLAST-BTM-Lite	commercial freeware (lite version)	NREL	Analysis and modeling of battery degradation
StorageVET	open source	EPRI	Optimization of size and financial evaluation of energy storage
SAM — System Advisor Model	BSD-3-clause	NREL	Modeling and analysis software for renewable energy projects
SimSES	BSD-3-clause	TUM	Physically motivated energy storage component, system and application behavior model

The storage value estimation tool[7] (**StorageVET**) developed mainly by the Electric Power Research Institute (*EPRI*) comes with a documentation, tutorial videos, and a user feedback forum. Since the release of version 2.0 the tool has been available as a Python package and most functional parts are licensed as 3-clause BSD open source. The tools allow conducting cost–benefit analysis and includes various application services like voltage support, retail demand charge reduction, frequency regulation, and even value stacking via aggregating multiple services to be served by one storage system. While the interface to the generation and storage technologies allows multiple options, at present only a very limited number of choices is available (PV/Internal Combustion Engine (ICE) and Battery/Compressed Air Energy Storage (CAES)). Furthermore, performance and degradation modeling is very limited, as it is based on an energy bucket model rather than analyzing the voltage and current specific phenomena of real world electro-chemical devices. Also, there is no thermal model included in the calculations, limiting the value of simulations for temperature sensible parameters like storage system efficiency (including Heating Ventilation Air Conditioning (HVAC) consumption) and storage aging.

Unlike the aforementioned tools, **SimSES** aims to bring together the model precision of tools like **SAM** and **PermodAC** and combine it with an interface to various applications and energy market scenarios. To do so, the model is distributed as open-source code on Gitlab[8] and Python Package Index[9] and builds up on a object-oriented approach programmed in Python language. Several modules are interlinked and interchangeable, and configuration files are used to select the setting of choice for typical time-series evaluations. The program as a whole, or parts of it, can also be integrated into simulation toolchains and modeling environments, making it feasible to be used in sensitivity and optimization studies and at the interface to a super-ordinate multi-instance controlling unit, as is further described in one of the case scenarios (Section 6.1). In order to allow the Energy Storage Systems (ESS) to react directly to states in a distribution grid, **SimSES** can be coupled to grid models, thus making it possible to have a power flow analysis and a detailed simulation of an ESS at the same time. **SimSES** stands out against above-mentionded tools, e.g., **Homer Pro** or **SAM**, by providing various detailed energy storage systems including validated and literature-based degradation models. Furthermore, a plethora of predefined storage-specific application Energy Management System (EMS) like ancillary services and energy trading are implemented and combined with suitable economic parameters, so that end-users are able to test a system of choice for a selected application use case. At the same time, the existent code framework is open-source accessible and open for future contributions from other developers worldwide.

3. Simulation framework for stationary energy storage systems

Stationary ESS may become a key component for future energy systems and incorporating various FTM and BTM applications supporting the electricity grid. Simulation tools are needed in order to provide advice for investment decisions and to analyze the impact of a stationary ESS. These tools should be able to model impact of applications on the health status of the ESS and its implications for prospective revenues.

While SimSES aims to allow for techno-economic cross-application and cross-technology comparisons, the tool is designed in a modular fashion and incorporates all technical components necessary for the grid connection of energy storage. Hence, **SimSES** does not only model various technologies, but also their thermal behavior, the corresponding power electronics, as well as the impact of different operating strategies. An integration into other energy simulation frameworks can be easily applied, as shown in project *openBEA*.[10]

The main task of **SimSES** is to determine the effects of the target power provided by the EMS regarding efficiency, temperature, and degradation of the ESS when applied to the storage system. Each implemented component is responsible for modeling its relevant principles. **SimSES** is divided into a simulation part for modeling the physical representation of the ESS and an evaluation part that provides technical and economic results as shown in Fig. 1. The figure also shows the basic working principle of **SimSES**: the time-series based simulation allocates an AC power target provided by the selected EMS to the storage system. After updating all models of the storage system, the current state regarding important variables such as SOC, temperature, SOH, and delivered power is transferred back to the operating strategy on which a new target power is calculated for the next time step.

In order to represent a storage system as a whole, various components need to be taken into account for a storage simulation. Besides the storage technology, power electronics is an important element. For instance, a simple Battery Energy Storage System (BESS) configuration consists of an Alternating Current to Direct Current (ACDC) converter connected to the grid and a battery. Additionally, stationary ESS are usually covered by a housing. These housings need to be thermally controlled in order to keep the ESS within its safety ranges. **SimSES** covers these possibilities with various configurable components and topologies.

More complex topologies can also include Direct Current to Direct Current (DCDC) converter or parallel connected ACDC converters, each connected to an ESS. Various ESS topologies are built with an AC connection to the grid or site location by connecting an ACDC converter to the storage system. However, in recent years Direct Current (DC)-coupled ESS has gained importance, especially in the residential

[7] https://www.storagevet.com/
[8] https://gitlab.lrz.de/open-ees-ses/simses
[9] https://pypi.org/project/simses/
[10] https://openbeaproject.wordpress.com/

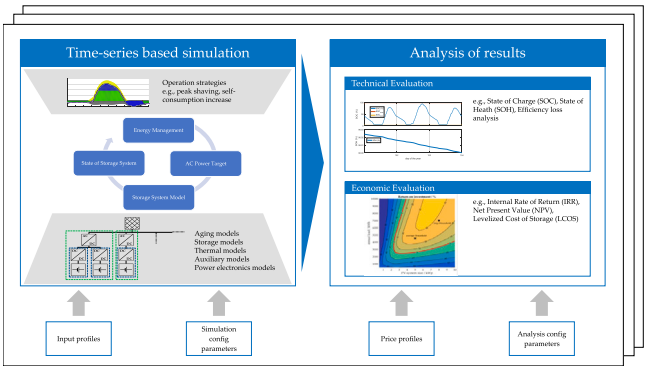

Fig. 1. Graphical overview of **SimSES** showing its simulation and analysis models, including the Energy Management System (EMS), storage system setup, technical and economical evaluation, and its necessary inputs. The state of a storage system includes the most important variables of the storage models, e.g., State of Charge (SOC), temperature, and State of Health (SOH).

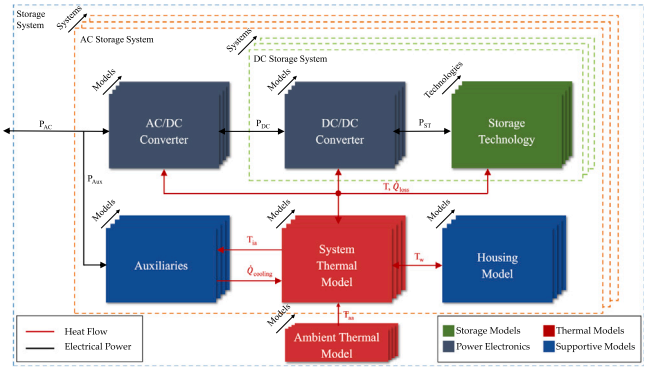

Fig. 2. Main component classes in **SimSES**: Interconnection of electrical and thermal models for ESS including the abstract AC and DC storage systems. Multiple model implementations exist for each component. Possible parallel connections of various AC and DC storage systems are indicated.

sector [19]. Hence, a state-of-the-art storage simulation framework needs to take varying topologies into account. **SimSES** considers these topologies by defining two abstract systems: AC and DC storage systems, which can also be combined in order to meet versatile topology configurations. Every AC storage system consists at least of an ACDC converter and a DC storage system. On the one hand, this allows the connection of several storage systems to the grid in parallel; on the other hand, this allows multiple DC-connected ESS within one storage system. Furthermore, the main ESS model is located inside the DC storage system behind a DCDC converter. These models are depicted in Fig. 2.

In the following sections, each of the **SimSES** packages as well as the underlying models and implementations are described in detail and shown in Fig. 3. *Storage Technology* and *System* provides models to represent physical models of storage system components while *Analysis* focuses on examining the simulation results regarding the technical and economical behavior of the simulated storage systems. All control algorithms and power flow management are handled within the *Logic* package.

Additional packages like *Commons*, *Simulation*, and *Data* deliver supportive functions for **SimSES**. *Config* is tasked to deliver functionality for the mentioned modular configuration of the ESS. In this package, software design patterns like the factory pattern are used to provide a wide range of configurable components [20]. Additionally, the structure allows the use of sensitivity analysis, e.g., by varying either different components or their dimensions. *Simulation* is another package that supports sensitivity analysis by allowing running multiple

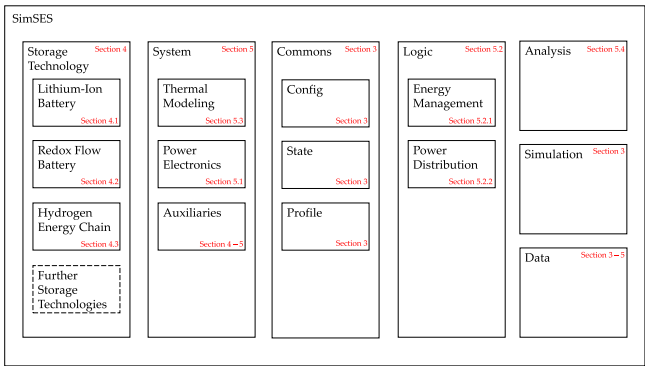

Fig. 3. Structure of **SimSES**: Packages are divided into *Storage Technology*, *System*, *Commons*, *Logic*, *Analysis*, *Simulation*, and *Data*. Within *Storage Technology*, the physical representation of each technology, namely LIB, RFB, and Hydrogen, is located. The *Commons* package delivers general functions for configuration and common features. The periphery is handled in the *System* package. Control algorithm and management is dealt with in the *Logic* package. *Analysis* focuses on the technical and economical evaluation of the simulation results. *Simulation* provides functions for simultaneous simulations, whereas *Data* stores all necessary information.

SimSES instances in parallel, therefore increasing simulation speed. For this purpose, Python's multiprocessing library is used. Further time series functions are implemented, like handling of profiles for power or price time series. These functions are used throughout **SimSES**, for example, by providing power profiles for the EMS. These supportive functions are covered within *Commons*, providing general functionality for time-series based simulations.

4. Storage technology models

Energy storage models represent the core of **SimSES**. In-depth models of various storage technologies are implemented, namely for LIB, RFB, and a hydrogen energy chain represented by electrolyzer, fuel cell and hydrogen storage. Each of these storage technologies have specific implementations regarding their physics and behavior. Due to the modularity of **SimSES**, further technologies can be implemented in future work.

4.1. Lithium-ion battery

ESSs based on LIB have evolved rapidly with a wide range of cell technologies and falling costs in recent years [11,21]. In **SimSES** LIBs are implemented as a distinct storage technology. The target power for this technology P_{st} depends on the storage structure and the power distributor as described in Section 5.

Four subcomponents are implemented in **SimSES** for behavior modeling of LIB. The **Equivalent Circuit Model (ECM)** is used to describe the electrical behavior of a specific cell type providing terminal voltage according to operational input data. The **Battery Management System (BMS)** monitors the cell operation conditions and updates values for the current. The electrical characteristics of LIBs in **SimSES** differ with chemistry and composition of constituent materials and may be fed with predefined manufacturer-specific datasets. Furthermore, various cell-specific degradation models can be selected in **SimSES**. The **aging** calculation is based on the cycle detector selected (e.g., half-cycle detector). These four main components are schematically illustrated in Fig. 4, and explained in detail in the following subsections.

4.1.1. Equivalent circuit model

To describe the electrical behavior, in **SimSES** the battery is implemented as a single-cell ECM. The currently implemented model includes an Open Circuit Voltage (OCV) and an internal resistance R_i, which is depicted in Fig. 4. According to Eq. (1), the terminal voltage

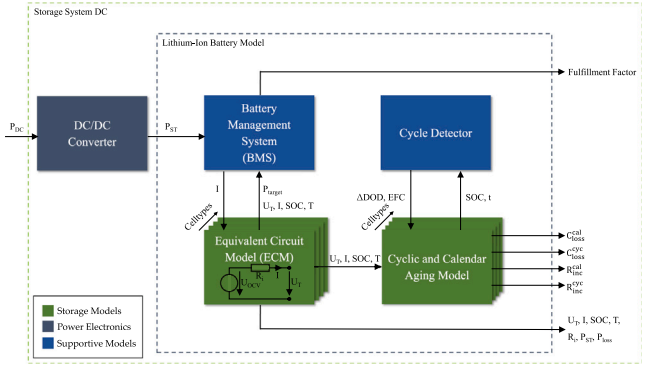

Fig. 4. Package structure of a lithium-ion battery. The battery package in **SimSES** includes four main components: a battery management system, a cell type including a equivalent circuit model, a degradation model, and a cycle detector.

U_T of each cell is calculated from the OCV and the voltage drop ΔU across R_i, due to the cell current I.

The OCVs of all currently implemented cell types are only dependent on the SOC but could be extended with further parameters like temperature and SOH. The internal resistance R_i of all currently implemented cell types takes the cell temperature T_{cell}, I, and the SOC into consideration. For both the SOC as well as R_i, the required data for different cell types are stored as look-up tables in **SimSES**. In between the available data points a linear interpolation is executed. Hence, the result quality relies on the number of data points. To improve performance, the interpolation of the SOC data was replaced by a fitted mathematical function, which is explained in Appendix A.

$$U_T = U_{OCV} - \Delta U = U_{OCV}(SOC) - I \cdot R_i\left(SOC, I, T_{cell}\right) \quad (1)$$

4.1.2. Battery management system

The BMS is linked to the ECM and is responsible for maintaining critical cell parameters within their permissible ranges. In addition to the target power P_{target}, voltage U_T, temperature T_{cell}, SOC, and current I are further input parameter for the BMS. According to the cell-specific parameters (e.g., maximum temperature), the BMS checks the input parameters and indicates whether they are within their limits. If limit violations occur, the current is restricted and returned to the ECM. The other parameters are recalculated accordingly and passed on to the aging models. The fulfillment factor indicates the share of the output power to the target power and will become sub-unity for simulations with boundary violations.

As seen in Eq. (1), the current I and the terminal voltage U_T are interdependent. Differential equations are necessary for calculating these values in the discrete time domain. To avoid these computationally intensive differential equations, an iteration loop is integrated in **SimSES**: the updated current I and terminal voltage U_T are iteratively derived through repetitive numerical approximation. This loop terminates after a predefined maximum number of iterations or as soon as the change in the current I or the terminal voltage U_T falls below a preset limit.

4.1.3. Lithium-ion battery cell types

The LIB cell forms the core of the BESS, and is essential for understanding the electrical and thermal characteristics of an entire system. For a more detailed discussion the reader is referred to [22,23] and for a description of current and future materials for LIBs as well as beyond lithium-based anode materials the reader is referred to [24]. In **SimSES**, three state-of-the-art technologies based on a Carbon-Graphite (C) anode and various cathode materials are currently implemented: two cells with a Nickel-Manganese-Cobalt-Oxide (NMC) cathode and one cell, each with a Lithium-Iron-Phosphate (LFP) and Nickel-Cobalt-Aluminum-Oxide (NCA) cathode, respectively. In addition, a generic cell with linear OCV is implemented in order to run simulations independent of the cell chemistry. Table 2 gives an overview of these cells, including their electrical attributes. The thermal parameters are summarized in Appendix B.

4.1.4. Lithium-ion battery degradation models

LIBs are subject to degradation due to multiple cell-internal aging processes, which can have significant impact on the economics of a BESS project [30]. In **SimSES**, degradation is modeled following a semi-empirical superposition approach of cyclic and calendar aging, as shown in Eqs. (2) and (3).

$$C_{loss}^{total} = C_{loss}^{cal} + C_{loss}^{cyc} \quad (2)$$

$$R_{inc}^{total} = R_{inc}^{cal} + R_{inc}^{cyc} \quad (3)$$

The resulting capacity loss C_{loss}^{total} and resistance increase R_{inc}^{total} are calculated through the addition of the respective calendar aging (C_{loss}^{cal}, R_{inc}^{cal}) and cyclic-aging components (C_{loss}^{cyc}, R_{inc}^{cyc}). Table 3 provides an overview of the primary LIB degradation models that are available in **SimSES** and their dependencies, as well as the sources on which these models are based. Here, t, SOC, T_{cell}, and U_T refer to the simulation time, state of charge, cell terminal voltage, and cell temperature, respectively. ΔDOD, EFC, Q, and $\overline{U_T}$ refer to the delta in depth of discharge for a cycle, the number of equivalent full cycles, the charge throughput, and the average cell terminal voltage over one equivalent cycle. The delta in depth of discharge (ΔDOD), as it is implemented here, is also referenced as depth of cycle or cycle depth in literature by some authors.

While calendar aging is computed once every simulation step, the model routine to calculate increase in cyclic aging is only triggered following the detection of half an equivalent cycle of charge throughput. This decreases the calculation time and allows determining the C-rate as well as DOC for that half equivalent cycle.

4.2. Redox flow battery

Large-scale storage systems are purportedly to be of rising concern in order to ease the growing penetration of RES. Hence, RFBs are of particular interest for multiple hour- and large-scale stationary ESSs because they can be easily and efficiently scaled according to the needs and become cost competitive at an energy range of multiple MWh [31]. To analyze their potential in different applications from small-scale (e.g., residential storage) to large-scale applications (e.g., industrial storage), they are integrated into **SimSES** as an additional storage technology. In an RFB, the liquid storage medium (electrolyte) is stored in external tanks. To charge and discharge the RFB, the electrolyte is pumped through a stack where the electrochemical reactions take place. The electrolyte divided in anolyte and catholyte solutions are separated by an ion-exchange membrane through which the charge carriers are transported. There are several known possible electrolyte combinations, e.g., all-vanadium or vanadium/bromine solutions [32]. As the energy conversion unit and the energy storage medium are decoupled, the power and energy of an RFB can be scaled separately [31,32].

Fig. 5 shows the structure of the main components modeled in **SimSES** to describe an RFB. The electrochemical model calculates the electrical operating parameters of a specific stack module dependent on the chemical composition of the selected electrolyte system. The control system checks whether the target parameters are within safe operating limits and returns the actual usable values. Different pumps and pump control algorithms can be configured. In the following, the model components are described in more detail.

Table 2
Lithium-ion battery cells currently implemented in **SimSES**, including their electrical parameters.

Manufacturer Model	Acronym in **SimSES**	Anode Cathode	Nom. voltage (V) Voltage range (V)	Capacity (Ah)	C_{rate} Ch. (1/h) C_{rate} Dch. (1/h)	Source
Sony[a] US26650FTC1	SonyLFP	Graphite $LiFePo_4$	3.2 2.0–3.6	3.0	1.0 6.6	[25,26]
Panasonic NCR18650PD	Panasonic- NCA	Graphite $LiNiCoAlO_2$	3.6 2.5–4.2	2.73	0.5 3.5	[27]
E-One Moli Energy IHR18650A	MolicelNMC	Graphite $LiNiCoMnO_2$	3.7 3.0–4.25	1.9	1.05 2.1	[28]
Sanyo UR18650E	SanyoNMC	Graphite $LiNiCoMnO_2$	3.6 2.5–4.2	2.05	1.0 3.0	[27,29]
Generic cell model	GenericCell	–	3.5 3.0–4.0	2.5	2.0 2.0	–

[a]Murata Manufacturing Co. acquired the Sony battery division in 2017.

Table 3
LIB-specific degradation models along with corresponding variable dependencies and literature sources.

Cell acronym	Calendar aging		Cyclic aging		Model based on
	C_{loss}^{cal}	R_{inc}^{cal}	C_{loss}^{cyc}	R_{inc}^{cyc}	
SonyLFP	t, SOC, T_{cell}	t, SOC, T_{cell}	EFC, ΔDOD, C-rate	EFC, ΔDOD, C-rate	[25,26]
PanasonicNCA	t, U_T, T_{cell}	t, SOC, T_{cell}	EFC, U_T, C-rate	EFC, U_T, C-rate	[27]
MolicelNMC	t, SOC, T_{cell}	t, SOC, T_{cell}	Q, ΔDOD, C-rate	Q, ΔDOD, C-rate	[28]
SanyoNMC	t, U_T, T_{cell}	t, U_T, T_{cell}	Q, ΔDOD, $\overline{U_T}$	Q, ΔDOD, $\overline{U_T}$	[29]
GenericCell	t	–	EFC	–	–

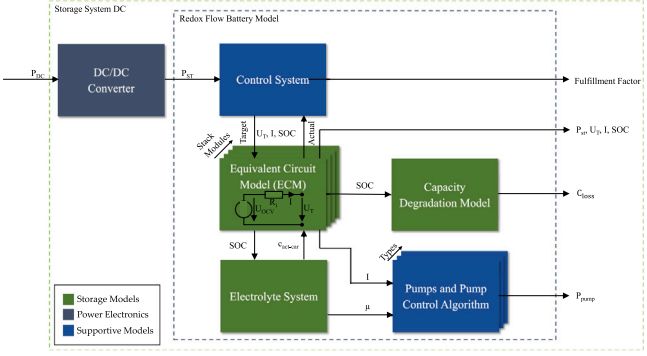

Fig. 5. Package structure for a redox flow battery (RFB). It contains an electrochemical model (equivalent circuit model) with specific parameters for different stack modules, an implemented control system, an electrolyte system, a degradation model, and pumps, with interchangeable control algorithms.

4.2.1. Electrochemical model

As with LIB, the currently implemented electrochemical model of an RFB is based on an equivalent circuit model (cf. Fig. 5). The terminal voltage U_T is directly calculated from the power applied to the RFB. Eq. (4) can be derived from Eq. (1) by using the relation between storage power P_{st}, terminal voltage U_T, and current I ($P_{st} = U_T \cdot I$). U_T is therefore calculated by P_{st}, the OCV, and the internal resistance R_i. Both OCV and R_i are dependent on the SOC and the electrolyte temperature in the stack module T_{stack}.

$$U_T = 0.5 \cdot \left(U_{OCV} + \sqrt{U_{OCV}^2 + 4 \cdot R_i \cdot P_{st}} \right)$$
$$U_{OCV} = f\left(SOC, T_{stack}\right) \quad (4)$$
$$R_i = f\left(SOC, T_{stack}\right)$$

Charge effects are taken into account by implementing a current for the charging losses $I_{char\text{-}loss}$ when calculating the change of the system SOC (SOC_{system}) via Eq. (5), considering the simulation time step Δt, the nominal voltage at the stack module U_{nom}, and the total energy of the electrolyte E_{total}. $I_{char\text{-}loss}$ includes coulombic losses due to self-discharge through the transport of reactants over the membrane and shunt currents. Shunt currents occur due to a connection of cells in the stack through an ionic conductive electrolyte distribution system. This creates a bypass current forced by the electric field due to the electrical series connection of the cells [33].

$$\Delta SOC_{system} = \frac{\left(I - I_{char\text{-}loss}\right) \cdot \Delta t \cdot U_{nom}}{E_{total}} \quad (5)$$

A control system is integrated in the electrochemical model, which checks whether U_T, I, and SOC are within safe operating limits. If the values are out of range, they will be adapted and the other parameters are recalculated accordingly.

Additionally, a capacity degradation model including the capacity losses C_{loss} due to hydrogen evolution is implemented in the RFB model. Further research is required to estimate a realistic hydrogen evolution current for industrial-sized stacks to predict the capacity reduction realistically over time. A current approach using experimental data of a laboratory cell from Schweiss et al. [34] overestimates the resulting capacity losses. Whitehead et al. [35] stated a capacity loss of less than 1% per year due to hydrogen evolution. Therefore, a hydrogen current of $5 \cdot 10^{-8}$ $\frac{mA}{cm^2}$ is assumed, resulting in a capacity loss of about 1% per year for a system with an Energy-to-Power Ratio (EPR) of 1. As the EPR increases, the loss decreases accordingly.

4.2.2. Stack module and electrolyte system

The calculations in the electrochemical model are based on electrical and geometrical data for a stack. A stack consists of a fixed number of cells electrically connected in series. The data to consider the voltage, charge, and hydraulic losses of a stack can be obtained either from experimental data or from the literature values and models. Stacks can be electrically connected in parallel or in series to a stack module to increase power and voltage of the RFB system. In this configuration the electrolyte flows in parallel through all cells and stacks. The performance parameters of the stack are directly connected to the used electrolyte system. The currently in **SimSES** examined and implemented electrolyte is an all-Vanadium system, consisting of 1.6 mol/l Vanadium solved in an aqueous sulfuric acid (2 mol/l H_2SO_4) from GfE (Gesellschaft für Elektrometallurgie mbH). To reduce side reaction due to high potentials and to prevent performance penalties the electrolyte needs to operate in a limited SOC range. A typical usable SOC range for a RFB lies between 20 and 80% [36]. Based on this SOC

Table 4
Redox-flow battery stack types in **SimSES**.

Acronym in SimSES	Cell number	Cell area (cm^2)	Based on experimental data of	Model based on
CellDataStack5500W	40	2160	Appendix C	[37–39]
DummyStack3000W	20	1000	N/A	N/A
IndustrialStack1500W	18	551	Voltstorage GmbH	[37,38]

range the nominal power of a stack is calculated. An overview of the in **SimSES** implemented stacks is listed in Table 4. The name of the stack includes its nominal power. In addition, some modifications of the described stacks are included, which are up-scaled or simplified versions that are not included in the list.

4.2.3. Pumps and pump control algorithm

The pump control algorithm used to control the flow rate or pressure drop in the system is an important performance-determining factor that affects the operating losses. Two different algorithms to choose from are currently integrated: the constant and the stoichiometric flow rate. It is assumed that the pumps always stop during stand-by to reduce the operating losses. If flow rate $\dot{V}$ or pressure drop Δp is given, the other value is calculated via Eq. (6) from the specific hydraulic, viscosity-corrected resistance $R_{hydraulic,specific}$ and the viscosity μ of the anolyte or catholyte.

$$\Delta p = \dot{V} \cdot R_{hydraulic,specific} \cdot \mu \tag{6}$$

If the pump is operating with a constant flow rate, it must be ensured that the volume flow is sufficiently high so that the stack module is supplied with enough reactants at any time of operation (depending on SOC and I). This is checked by the control system integrated in the electrochemical model.

For the stoichiometric flow rate algorithm $\dot{V}$ is calculated according to Eq. (7) via the stoichiometric factor ν, the total concentration of the active charge carriers in the electrolyte $c_{act\text{-}car}$ (for the implemented Vanadium electrolyte it is 1.6 mol/l), the Faraday constant F, and the still available concentration of reactants in the electrolyte, which is described through the SOC for discharging and (SOC − 1) for charging. If, for example, the RFB is charging at SOC 70%, reactants that can be maximal charged in the Stack are 30% of the total concentration, therefore value is 0.3.

$$\begin{aligned} \dot{V} &= \frac{\nu \cdot I}{F \cdot c_{act\text{-}car} \cdot (SOC - 1)} \quad \text{for} \quad P >= 0 \\ \dot{V} &= \frac{\nu \cdot I}{F \cdot c_{act\text{-}car} \cdot SOC} \quad \text{for} \quad P < 0 \end{aligned} \tag{7}$$

The pump losses P_{pump} can be calculated with Δp, $\dot{V}$, and the pump efficiency η_{pump} of a specific pump that can be selected in **SimSES** via Eq. (8) [40].

$$P_{pump} = \frac{\dot{V} \cdot \Delta p}{\eta_{pump}} \tag{8}$$

4.3. Hydrogen energy chain: Electrolyzer, storage, and fuel cell

Hydrogen as an energy carrier is supposed to be one of the major contributors impacting future energy provision, storage, and distribution [41]. The abundance of chemically-bound hydrogen in the form of water as well as its very high-energy density is compelling for its deployment as an energy carrier for large-scale energy storage. However, the efficiency of splitting water into its separate components via electrochemical electrolysis and reverting the process through fuel cells or combustion power plants is comparatively low, in striking contrast to electrochemical storage like LIB [14,42]. As such, hydrogen is thought to complement rather than to compete with LIB and RFB. In order to understand the effects of a hydrogen-based energy chain on a system level including its periphery, models for *electrolyzers*, *fuel cells*, *hydrogen storage*, and its auxiliary components like pumps and compressors are integrated as models within **SimSES**. Within this section, implementations of the respective models are explained in detail.

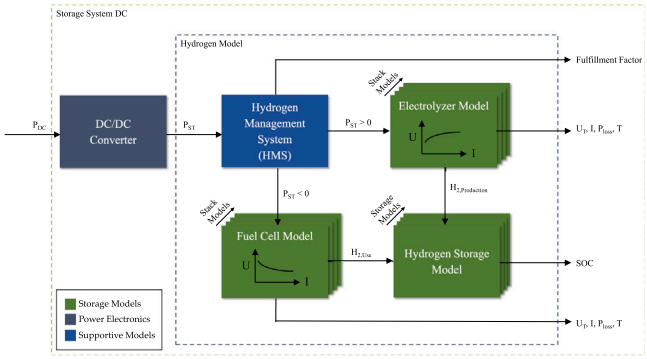

Fig. 6. Package structure for hydrogen in **SimSES** includes four main components: a *hydrogen management system*, an *electrolyzer*, a *fuel cell*, and a *storage model*.

The hydrogen package structure is displayed in Fig. 6, consisting of a *Hydrogen Management System (HMS)*, an *electrolyzer*, a *fuel cell*, and a H_2 *storage model*. The *HMS* supervises the whole hydrogen chain for valid ranges of temperature and SOC and reduces applied power if necessary. The storage model could be a gas pipe with an assumed infinite capacity or a hydrogen pressure tank with a predefined energy capacity. Depending on the pressure of the gas within the storage tank, the gas needs to be compressed to the desired pressure level. The *electrolyzer* and *fuel cell* models are explained in detail in the following sections. It is worth to mention that **SimSES** also allows a single-direction hydrogen energy chain by neglecting either the *electrolyzer* or the *fuel cell* component with special implementations. A summary of all currently implemented models is given in Table 5. Due to the modular structure of **SimSES**, additional models can be implemented in a future release accordingly.

4.3.1. Electrolyzer

A water electrolyzer splits water with the use of electricity into hydrogen and oxygen by passing ions through an electrolyte from one electrode to the other. The pressure and temperature-dependent polarization curve is based on the general equation of Nernst voltage U_{nernst} as well as overpotentials represented by ohmic η_{ohm}, activation η_{act}, and diffusion losses η_{diff} as shown in Eq. (9) [50]. In some implementations mass transport and membrane permeation are also considered.

$$U_{T,EL} = U_{nernst} + \eta_{ohm} + \eta_{act} + \eta_{diff} \tag{9}$$

Depending on the stack technology, e.g., alkaline or polymer electrolyte membranes (PEM), the *electrolyzer* is operated at different pressure and temperature levels, which is taken into consideration by varying polarization curves for each technology [50]. As shown in Fig. 7, the *electrolyzer* model is divided into its stack and corresponding degradation models, pressure and thermal models as well as necessary auxiliaries like a pump, water heater, and gas dryer. The electrical auxiliary power is calculated according to the hydrogen and oxygen generation pressures for the anode and cathode, as well as the stack temperature. A water pump regulates the humidification of the *electrolyzer*, whereas the generated hydrogen gas needs to be dried. These auxiliary models calculate the necessary electrical power in order to provide a temperature and mass equilibrium.

Table 5
Overview of implemented *electrolyzer*, *fuel cell* and *hydrogen storage* models in **SimSES**.

Technology	Acronym in SimSES	Type	Degradation effects	Based on experimental data of	Model based on
Electrolyzer	PemElectrolyzerMultiDimAnalytic	PEM	Resistance increase, Decrease of exchange current	Forschungszentrum Jülich	[43–45]
	PemElectrolyzer	PEM	N/A	N/A	[46]
	AlkalineElectrolyzer	Alkaline	N/A	Hydrogen Research Institute	[47,48]
Fuel Cell	PemFuelCell	PEM	N/A	N/A	[49]
	JupiterFuelCell	PEM	N/A	SFC Energy AG	–
Hydrogen Storage	PressureTank	Pressure Tank	N/A	N/A	–
	SimplePipeline	Pipeline	N/A	N/A	–

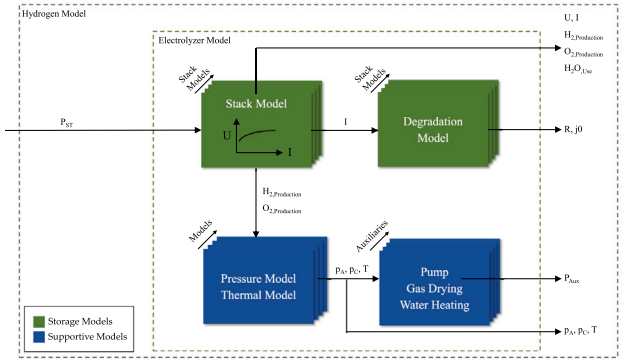

Fig. 7. Package structure for *electrolyzer* in **SimSES** includes a stack, pressure, thermal and degradation model as well as a pump and gas dryer.

Electrolyzer degradation is a field of ongoing research with controversy over underlying mechanisms and influencing factors [51,52]. However, active operation time and applied current density seem to be major impact factors for electrolyzer degradation. For instance, the implemented degradation for the Polymer Electrolyte Membrane (PEM) electrolyzer acquired from the work of Tjarks [43] is based on the findings of Rakousky et al. [44,45] considering a resistance increase and a decrease of the exchange current. Other implementations of electrolyzers are a PEM variant without degradation effects based on the work of Marangio et al. [46] and an alkaline version based on the work of Hammoudi et al. [47] and Henao et al. [48].

4.3.2. Fuel cell

As an opposite to *electrolyzers*, *fuel cells* combine hydrogen and oxygen to water while releasing usable energy in the form of electricity [42]. The terminal voltage is calculated by the Nernst voltage subtracted by the voltages due to ohmic, activation, and diffusion losses shown in Eq. (10).

$$U_{T,FC} = U_{nernst} - \eta_{ohm} - \eta_{akt} - \eta_{diff} \tag{10}$$

The *fuel cell* package has a structure that is similar to the *electrolyzer* package, with a stack, pressure, and thermal model. During operation, the water handling especially for PEM fuel cells is crucial and handled by water pumps. An implementation of a PEM fuel cell based on Feroldi et al. [49] as well as a model for the Jupiter PEM fuel cell of SFC Energy AG[11] including a thermal model is available in **SimSES**. However, the implementation of adequate degradation models within SimSES is a task for future action.

5. System periphery, management, and evaluation

Energy storage systems not only consist of the underlying storage technology but also the periphery like power electronic components and thermal behavior as well as an EMS. These elements are crucial for evaluating energy storage systems as a whole. In order to provide insights into the overall system behavior, **SimSES** not only models the periphery and the EMS, it also provides in-depth technical and economical analysis of the investigated ESS.

5.1. Power electronics

Besides the storage technology, the power electronic components play a crucial role in terms of system efficiency. Depending on topology and application, power electronics may contribute significantly to the overall system losses [53]. Hence, **SimSES** has to consider these electronic components for an accurate simulation of a storage system like ACDC and DCDC converters. An overview of the implemented models in **SimSES** is given in Table 6. Models of these converters are represented by power and voltage-dependent efficiency curves. In principle, the efficiency of a power electronics module is represented by a given storage power $P_{Storage}$ and the rated power of the power electronics component P_{Rated} as displayed in Eq. (11).

$$\eta_{PE} = f\left(P_{Storage}, P_{Rated}\right) \tag{11}$$

The power applied to the power electronic components is crucial for simulating the efficiency. When considering storage systems, it is possible that these systems do not fully deliver the requested power. These situations occur, for example, if the storage is outside of its temperature limits or the SOC is at its lower or upper limits. Hence, the power is adjusted compared to the target power of the EMS, which leads not only to non-fulfillment, but also to an altered efficiency.

5.2. Power control

Every power flow in an ESS has to be monitored and controlled. The power flow is dependent on the application and system topology. In **SimSES**, these two dependencies are handled separately with an EMS, respectively, Power Distribution Strategies (PDS). The EMS defines the target power for the ESS as a function of the application while the PDS allocates the target power to the configured subsystems. These control mechanisms are explained in detail in the following sections.

5.2.1. Energy management system

The EMS in an ESS is a system consisting of both hardware and software that allows the user to monitor and control the energy flows within an ESS. In **SimSES**, the function of the EMS is to calculate and supply a target power value for each simulation timestep (Δt) based on the selected operation strategy. This target power value can be dependent or independent of previous system states as well as interfere with various input profiles. In **SimSES** both stand-alone and stacked operation strategies can be simulated. Stacked operation strategies are sorted according to their user-associated priority level. Consequently, the individual stand-alone operating strategies are executed one after another depending on their priority. Additionally, time-discrete serial stacking is already available within **SimSES**. More complex multi-use strategies can be integrated as stand-alone strategies. At present, a handful of

[11] https://www.efoy-pro.com/efoy-pro/efoy-jupiter-2-5/

Table 6
Overview of implemented ACDC and DCDC converter models in **SimSES**.

Converter type	Acronym in SimSES	Based on experimental data of	Model based on
AC/DC	FixEfficiencyAcDcConverter	N/A	N/A
	NottonAcDcConverter	N/A	[54]
	Sinamics120AcDcConverter	Sinamics S120	[55]
	BonfiglioliAcDcConverter	Bonfiglioli RPS TL-4Q	Datasheet[a]
	SungrowAcDcConverter	Sungrow SC 1000 TL	Datasheet[b]
	M2bAcDcConverter	Stable Energy GmbH	[56]
DC/DC	FixEfficiencyDcDcConverter	N/A	N/A

[a] https://www.docsbonfiglioli.com.
[b] https://en.sungrowpower.com.

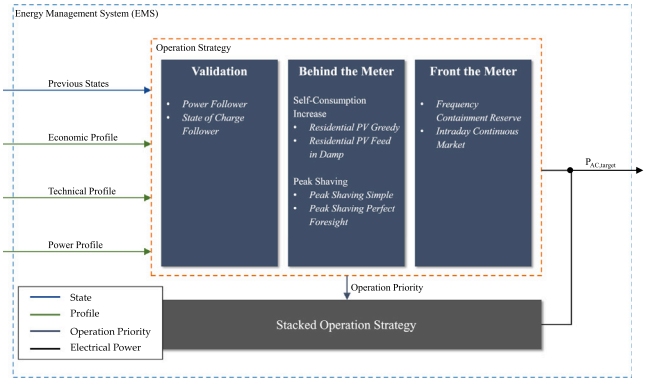

Fig. 8. Structure of the energy management system and overview of available operation strategies and their categorization in **SimSES**.

operation strategies are implemented in **SimSES**. An overview of these operation strategies and their categorization is depicted in Fig. 8.

The *power follower* strategy is a basic operation strategy which aims to get the storage system operation to replicate a given power profile. Similar to the aforementioned strategy, the *SOC follower* converts a given SOC profile to a power profile and attempts to make the storage system fulfill this calculated demand power at each timestep.

Based on the work of Zeh and Witzmann [57], two operation strategies for residential SCI in combination with Photovoltaic (PV) generation units have been implemented. The *residential PV greedy* operation strategy charges the ESS as fast as possible without consideration of the grid by meeting the residual load at all times. To reduce the maximum grid load the *residential PV feed in damp* operation strategy schedules the charging of the ESS according to a PV prediction. It attempts to provide a constant charging power and aims for a fully charged ESS at sundown.

Two strategies have currently been implemented for industrial consumers. The simple *Peak Shaving (PS)* strategy works as follows. As long as the target power is above a specified threshold, the additionally required power is provided by the ESS. In addition, the ESS will recharge itself if the power value is below the PS threshold [58] (used in the case study in Section 6.1). In order to reduce calendar aging for a lithium-ion based ESS, the *PS perfect foresight* strategy operates under the assumption of perfect foresight for the load profile. The ESS will only charge up to the energy that is required for the next load peak, right before the occurrence of that load peak [59].

The EMS strategy for providing *FCR* implemented in **SimSES** is based on the German regulatory framework [60,61]. The requested charging and discharging power is proportional to the frequency deviation. Below 49.8 Hz or above 50.2 Hz the output power is set to the prequalified power. Within the frequency dead band around 50 Hz with +/-10 mHz the output power is set to 0 W. The degree of freedom to exceed the output power by 20% is used, aiming to bring the SOC back to a predefined SOC set-point. The *IDM* operation strategy charges or discharges the ESS by trading energy on the electricity market, in particular on the IDM, if the SOC falls below a predefined lower limit or it exceeds an upper limit [62]. An example for a *FCR* and a *IDM* stacked operation strategy is provided in Section 6.2.

5.2.2. Power distribution strategies

For complex storage system topologies, the power needs to be distributed between the different subsystems of an ESS [63,64]. For this purpose, several power distribution logics are implemented in **SimSES**. These logics distribute the power to the corresponding storage systems, for instance, based on the respective SOH or SOC. In **SimSES**, the ESS is differentiated between an AC and DC storage system (see Section 3). For each node of parallel connected AC systems as well as DC systems, a power flow decision has to be made similar to Bauer [64]. Mühlbauer et al. [63] as well as Bauer [64] define PDS as a simple problem of a distribution factor α as shown in Eq. (12).

$$P_i = P_{target} \cdot \alpha_i, \tag{12}$$

where P_{target} is the target power provided by the EMS, α_i the power distribution factor for system i, and P_i the corresponding power of system i on condition that the sum of all α_i equals one. In an optimal case the PDS takes the current limitations of the underlying storage technology for P_i into consideration in order to be able to fulfill the requested power, e.g., temperature limitations could lead to lower deliverable power. For each node, a PDS can be configured.

Mühlbauer et al. distinguish between static and dynamic categories for PDS while Bauer has more subtle definitions for a dynamical PDS approach with a fixed and variable sequence [63,64]. Bauer also mentions a PDS as an optimization problem currently not considered in **SimSES**. In the following, PDS implemented in **SimSES** are presented.

The most straightforward implementation of a PDS is an equal distribution of the power to all storage systems. This is a static PDS approach with a fixed power distribution factor. Other static PDS-like distribution based on the ESS capacity can be easily added to the PDS set of **SimSES**. In addition, a dynamic PDS is implemented by differentiating between charge and discharge distribution factors depending on the SOC of each system based on [63].

Due to the modularity of **SimSES**, multiple ESSs with different storage technologies can be combined with a hybrid ESS, e.g., a LIB and a RFB system. For this purpose, a novel PDS is introduced prioritizing configured storage technologies by base and peak loads, respectively. While the prioritized system stays within a defined SOC range, e.g., between 25 % and 75 %, it tries to fulfill the target power within its power limits. If either the SOC or the power limit is exceeded, the next highest prioritized system takes over. If the power target is not completely allocated, a second loop distributes the power independent from the defined SOC range. In addition, the logic balances the SOC of the configured ESS if one or more systems are outside of the defined SOC range while other systems are within those ranges. The algorithm also allows a two or one way balancing, e.g., if only the peak load system should be balanced by the base load system (used in the case studies in Section 6).

5.3. Thermal modeling

Performance, efficiency, and aging of all aforementioned storage processes depend not only on charge and discharge currents, but are also highly sensitive to thermal conditions. While for some small-scale storage realizations (e.g., residential battery storage) modeling electricity flows in a fixed temperature setting might be a solution of choice with sufficient accuracy for techno-economic simulations [65], larger storage systems along with investigations about storage efficiency particularly require detailed thermal models [53]. Utility-scale LIB stationary ESS are often designed as free-standing systems, which are installed outdoors and exposed to the environment. The use of standard shipping containers to install entire energy storage systems is the preferred option in the industry today to shield sensitive electric components from adverse environmental conditions. The benefits of such a configuration include modularity, scalability, ease of logistics, conformance with road-transport regulations, and the ability to plan and optimize land usage. Such containers are also specially fitted out with insulation to limit heat flow to/from the environment, and to present a stable operation temperature to the components inside.

Heat is generated in LIBs due to internal resistance to the passage of current during operation. Lithium-ion cell technology is particularly vulnerable to adverse changes in cell temperatures, and degrade faster when operated outside of their optimal temperature ranges. In particular, degradation may result from accelerated kinetics for unwanted side reactions at elevated temperatures resulting in a loss of capacity and an increase in the internal resistance. If the generated heat is not rejected to the environment at a rate greater than the rate of heat generation, overheating and—in extreme cases—a *thermal runaway* may occur. In contrast, for applications with relatively lower current rates (alike most stationary storage use cases), air cooling systems are deemed adequate to aid the heat rejection process to maintain the cell temperatures within the stipulated ranges. It is worth to mention in this context, that in the absence of cooling systems, the capabilities of the cells are severely limited, and under-utilized [66].

In summary, thermal modeling of energy storage systems is a crucial step of the system design process, especially due to the following factors:

- temperature-dependence of the energy conversion efficiency of LIB (dependent on the internal resistance) [67] and other storage technologies,
- temperature-dependence of the degradation mechanisms [68,69],
- dependence of the round-trip efficiency on the energy consumption of auxiliary components, such as the HVAC system [55] and
- operational hazards under extreme temperatures which are too low, or too high [70].

Thermal modeling in **SimSES** follows a zero-dimensional lumped-capacity approach, and consists of a number of component packages which run in tandem to emulate the thermal behavior of a system under the specified operating conditions. Zero-dimensional lumped-capacity approaches are widely used in the reviewed literature and found to be suitable for system models [55,71]. Each of these packages and their core features are presented in this section, along with how they fit into the larger picture within **SimSES** and its architecture. The thermal model and its associated components function at the AC storage system level in **SimSES**. **SimSES** currently supports a container-based housing solution with an air cooling system for LIB stationary ESS. An overview of these packages and their interplay is seen in Fig. 9.

5.3.1. Ambient thermal model

The primary function of the ambient thermal model is to account for the predominant environmental effects that play a role in the thermal behavior of the ESS. The ambient thermal model currently consists

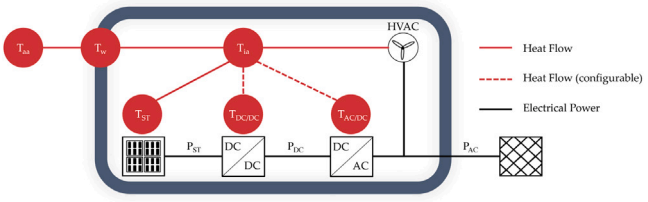

Fig. 9. SimSES is thermally interconnected with the thermal nodes of ambient air T_{aa}, wall T_w, inner air T_{ia}, and storage technology T_{ST}. The temperature conjunction of T_{ACDC} and T_{DCDC} can be switched off. The HVAC system controls T_{ia} of the storage system.

of an ambient temperature which supplies a value of ambient air temperature T_{aa} for each simulation timestep Δt at time t. The ambient temperature is available in two variants: a constant temperature model, which supplies a user-specified T_{aa} for each timestep, and a location-specific model, which, depending on the time of day and year, supplies a value of T_{aa} based on recorded temperature time-series data. The ambient temperature datasets currently present in SimSES have been generated with the help of the publicly available simulation tool *greenius*, developed by the German Aerospace Center (DLR) [72]. A solar irradiation model is also envisioned for a future release of SimSES as an extension of the ambient thermal model in order to be able to supply values of incident solar irradiation at a given location at time t to allow for better estimation of the heat load on an ESS. The ambient thermal model is understandably applicable to all AC storage system instances present in a given BESS configuration.

5.3.2. Housing model

The housing model emulates the physical attributes of the specified housing type. **SimSES** currently supports system simulations with a standard 20 foot shipping container as the housing. The walls are modeled with three layers of materials, including an insulating layer of Polyurethane (PU) between the outer and inner metal layers. The geometrical dimensions and physical and thermal properties of the walls of the shipping container can be adapted to suit any desired variant. The modular and extendable structure of **SimSES** ensures that the choice is not limited to the presently implemented model, but rather allows for other housing types or installation conditions to be modeled and included in simulations.

5.3.3. Heating, ventilation and air conditioning model

As the temperature inside the housing is to be maintained within a stipulated range to ensure safe and optimal operating conditions, a HVAC unit is necessary to correct temperature deviations. **SimSES** also supports inclusion and modeling of HVAC systems. Two basic HVAC models are currently implemented: one, which uses the internal air temperature T_{ia} deviation from its user-specified set-point to roughly estimate the amount of thermal power required to counter this deviation, and the other, which employs a Proportional-Integral-Derivative (PID) controller logic to arrive at a value of thermal power to counteract the deviation in T_{ia} from its set-point. The corresponding electrical power consumption $P_{electrical}$ of the HVAC, which is related to the thermal power P_{hvac} by the Coefficient of Performance (COP) (see Eq. (13)), is logged in the state of the AC storage system, and influences the round-trip efficiency of the ESS.

$$P_{electrical} = \frac{P_{hvac}}{COP} \tag{13}$$

5.3.4. System thermal model

The system thermal model is central to the thermal modeling process in **SimSES**, in that it emulates the physical phenomenon of heat transfer among the components of the ESS and its environment, as well as integrates the functioning of all aforementioned components. The

system thermal model estimates the temperatures of all components of interest after each simulation timestep Δt, based on the various heat loads—both external and internal—that the ESS is subjected to. Each instance of AC storage system has its own system thermal model, and captures the thermal behavior of all components present in each AC storage system. The analysis applies the zero-dimensional lumped capacity approach, and the central assumption is that all the components are treated as lumped isotropic homogeneous objects with heat capacities and heat transfer coefficients. The internal air in the container is assumed to possess a uniform temperature throughout its volume, and flows are not considered. The temperatures of the storage technologies influence important parameters such as efficiency and voltage, as well as the rate at which they degrade. The component models used in **SimSES**, which are explained in the subsequent sections, take these temperature variations into account.

The system thermal model solves a system of first-order coupled differential equations to obtain the temperatures of the storage technologies, the internal air, and components such as the ACDC converter, if they are present within the same housing. This list of components, whose temperatures are of interest, can be expanded as required owing to the modular structure of the system thermal model. As the temperatures at the start of each timestep Δt are known, and the temperatures at the end of each timestep are of interest, an initial value problem can be formulated.

Within each DC storage system, for each instance of storage technology *i* with a mass m_{st} and specific heat c_p^{st}, a differential equation capturing the variation in its temperature T_{ST} under the combined effects of natural convection with the internal air (ia) P_{conv}^{st-ia} and the heat generation within itself on account of energy conversion losses P_{loss}^{st} can be formulated (see Fig. 9). For an AC storage system with a total of *n* storage technology instances within its DC storage systems, a total of *n* differential equations based on Eq. (14) can be formulated.

$$m_{st,i} \cdot c_p^{st,i} \cdot \frac{dT_{st,i}}{dt} = P_{loss}^{st,i} - P_{conv}^{st,i-ia} \tag{14}$$

Similarly, a heat balance equation with a form similar to Eq. (14) can be formulated for other components such as the ACDC converter, which also introduce heat into the housing due to the energy conversion losses (see Fig. 9).

For the internal air with a mass m_{ia} and specific heat c_p^{ia}, a heat balance can also be formulated to determine the variation in its temperature T_{ia}. The heat balance outlines its interaction via natural convection with each storage technology P_{conv}^{st-ia}, other components such as the ACDC converter (if present) $P_{conv}^{acdc-ia}$, and the innermost layer (il) of the housing walls P_{conv}^{il-ia}. The thermal power of the HVAC P_{hvac} is also accounted for in this balance (see Eq. (15)).

$$m_{ia} \cdot c_{p,ia} \cdot \frac{dT_{ia}}{dt} = \Sigma P_{conv}^{st,i-ia} + P_{conv}^{acdc-ia} - P_{hvac} - P_{conv}^{ia-il} \tag{15}$$

The innermost layer of the housing walls, in addition to the convective heat transfer with the internal air, also exchanges heat with the insulation layer adjacent to it via heat conduction, and a heat balance equation can be written.

The insulation layer interacts with both the innermost and outer layers via heat conduction, and a corresponding heat balance equation can be drafted as well. The outer layer exchanges heat with the adjacent insulation layer via conduction, and interacts with the ambient air via natural convection. The outer layer is also subjected to a heat load due to the direct and diffuse solar irradiation incident on its surfaces. A heat balance for the outer layer can be applied by taking into account the heat loads due to the incident solar irradiation, the conduction through the layers, and the natural convection with the ambient air.

Depending on the chosen simulation timestep Δt, the heat balance equations for all considered components are then solved simultaneously at least once, or in the case of very large Δt, the system of equations is solved multiple times in an attempt to obtain a greater degree of accuracy. The solution of this system of equations yields the values of the temperatures at the end of each simulation timestep, which influence the component models.

In case simpler simulations are to be conducted, the thermal model can also be disabled, in which case the storage technologies experience a constant (user-defined) ambient temperature, and the temperatures of the storage technologies and other components are also set to remain at this value and are not updated. **SimSES** currently only offers modeling of thermal behavior for LIB. Augmentation of these capabilities for other storage technologies is planned for future releases.

5.4. Analysis

Following the simulation of ESSs, an analysis of the simulation results is conducted automatically by **SimSES** providing Key Performance Indicators (KPIs) and plots that allow the user to gain insights of the configured ESS. Furthermore, the analysis can be used to compare simulation results of different scenarios quantitatively and qualitatively. While the *Data* subpackage provides relevant parsers and utility functions for processing the time series of simulation results, the *Evaluation* subpackage includes the actual methods for deriving the KPIs and creating plots. Which evaluations should be performed, as well as relevant input data (e.g., electricity prices and storage cost) can be specified by the user. In the following, the technical evaluation and economic evaluation will be explained in more detail.

5.4.1. Technical evaluation

Within the *Technical Evaluation* part of **SimSES**, technical KPIs are determined on the system and storage technology level. Depending on the storage technology used, the respective KPIs are exported at the end of the analysis. Automatically generated plots give the user an impression of the usage and performance of the simulated ESS like time variance of AC and DC power, SOC and capacity. More advanced users can also use the simulation results to calculate characteristic values beyond the displayed KPIs. The technical evaluation's KPIs on system, lithium-ion, redox flow and hydrogen level are summarized in Table 7. As an example, the calculation of two KPIs is shown below.

The Round-Trip Efficiency (RTE) is calculated on the system level using Eq. (17) deviated from Eq. (16). To calculate the RTE, the discharged energy (E_{out}) is divided by the charged energy (E_{in}), from which the change of energy by SOC rise or decrease (ΔE) is subtracted. For simulations over a longer period of time, the efficiency influence on the SOC change can be neglected because charged and discharged energy are substantially larger than the change in energy between the start and end SOC of the simulation. For shorter simulation periods, the influence of efficiency on the SOC change must be considered. For this purpose, the SOC change is divided by the root of the efficiency, since, for example, the additionally charged energy at SOC increase has already passed through the power electronics in one direction and was thus influenced by the efficiency. A symmetrical efficiency for charge and discharge is assumed here.

$$\eta_{RTE} = \frac{E_{out}}{E_{in} - \frac{\Delta E}{\sqrt{\eta_{RTE}}}} \tag{16}$$

with $\Delta E = SOC_{last} \cdot E_{last} - SOC_{initial} \cdot E_{initial}$. Solving Eq. (16) for η_{RTE} leads to:

$$\eta_{RTE} = \frac{E_{out}}{E_{in}} + \frac{\Delta E^2 + \Delta E\sqrt{4E_{out}E_{in} + \Delta E^2}}{2E_{in}^2} \tag{17}$$

Another KPI calculated in the technical analysis is the remaining energy content (e_{rem}) as a percentage of the initial energy (Eq. (18)). For this, the current energy (E_{act}) is divided by the initial energy (E_{nom}).

$$e_{rem} = \frac{E_{act}}{E_{nom}} \tag{18}$$

Table 7
Key Performance Indicators (KPIs) for technical evaluation and the level at which they are calculated. Crosses indicate for which level the respective KPI is calculated.

Selected key performance indicators (KPI)	System	Lithium-ion	Redox flow	Hydrogen
Round-trip efficiency (%)	x	x	x	x
Mean state of charge (%)	x	x	x	x
Number of changes of signs per day (#)	x	x	x	x
Avg. length of resting times (min)	x	x	x	x
Pos. energy between changes of sign (% of capacity)	x	x	x	x
Avg. fulfillment factor (%)	x	x	x	x
Remaining capacity (%)	x	x	x	x
Energy throughput (kWh)	x	x	x	x
Mean power electronics efficiency (%)	x			
Equivalent full cycles (#)		x	x	
Depth of discharges (%)		x	x	
Coulomb efficiency (%)			x	
State of health (%)				x
Energy for heating of water (kWh)				x
Energy for compression of hydrogen produced (kWh)				x
Total mass of hydrogen (kg)				x

5.4.2. Economic evaluation

The economic evaluation of **SimSES** allows assessing the overall profitability of an energy storage project through economic KPIs. These KPIs include the net present value (NPV), internal rate of return, profitability index, return on investment, and levelized cost of storage. Eq. (19) shows the calculation of the NPV as it is performed in **SimSES**.

$$\mathrm{NPV} = -\mathrm{I}_0 + \sum_{\mathrm{n}=1}^{\mathrm{N}} \frac{\mathrm{CF}_\mathrm{n}}{(1+\mathrm{i})^\mathrm{n}} \tag{19}$$

I_0 denotes the initial investment cost, i the discount rate, CF the cashflow, and n and N the current and total number of project years, respectively. All parameters apart from the cashflow are derived from the settings in the Configuration File. The cashflow itself is calculated from the time series of logged simulation results. Depending on the selected operation strategy, the cashflows of multiple revenue streams ($\mathrm{CF}_{\mathrm{n,r}}$) may be added to obtain the cashflow for a single project year (CF_n), as shown in Eq. (20).

$$\mathrm{CF}_\mathrm{n} = -\mathrm{OM}_\mathrm{n} + \sum_{\mathrm{r}\in\mathrm{R}} \mathrm{CF}_{\mathrm{n,r}} \tag{20}$$

Here, R denotes the set of applicable revenues streams r for the selected operation strategy and OM the operation and maintenance cost. Table 8 shows the matching of revenue streams and operation strategies, while the following list provides brief descriptions for all currently implemented revenue streams. For stacked operation strategies, such as *FCR* paired with *IDM*, all respective revenue streams will be considered in Eq. (20).

- *Energy Cost Reduction (ECR)*: Reduction of energy-based electricity costs, caused, for example, by increased self-consumption of PV-generated electricity. This is calculated based on the total site load for both with and without the BESS, the electricity purchase price, and the electricity sales price or feed-in tariff.
- *Demand Charge Reduction (DCR)*: Savings generated by a reduction in demand charges, calculated based on the maximum site load with and without the BESS, the applicable billing period, and the demand charge price per unit of power.
- *Frequency Containment Reserve (FCR)*: Revenue that is generated by participating in the FCR market, calculated based on the system's nominal power, the FCR price, and the power allocated to the FCR market.
- *Spot Market Trading (SMT)*: Revenue that is generated through spot market trading, based on the amount of energy traded and the specified time series of prices.

6. Case studies

The following section will focus on **SimSES** from a user perspective. Compared to other solutions and tools in the field of energy system simulation, **SimSES** provides detailed modeling of ESS and applications on a system level during the full investment period. Both the technical properties of different storage technologies and the economic modeling of the components and systems are mapped in detail.

In order to clarify the implementation and adaptability of the tool, two applications are discussed. First, Peak Shaving (PS) for an industrial application comparing a different set of storage technologies—LIB, RFB, and a hybrid system of both technologies. Second, Frequency Containment Reserve (FCR) including an Intraday Continuous Market (IDM) by considering various system topologies are discussed. The underlying system costs are discussed in Appendix D. These case studies can be downloaded and executed as described in Appendix E.

6.1. Case study 1: Peak shaving application

A commonly used application for ESS is Peak Shaving (PS). The tariff model with separate energy- and power-related prices plays an important role here. The PS application aims to cut high power demands from the distribution grid. Since the highest power peak per billing period (usually monthly or annually) is multiplied by the power-related price, it can be economical favorable to cap high demand peaks by using an ESS to provide the necessary power and energy [9].

In this case study, three different storage systems are simulated: a LIB system with 150 kWh, a RFB system with 200 kWh, and a hybrid system with 10 kWh LIB capacity and 180 kWh RFB capacity. More detail on the system configuration chosen for this case study is given in Fig. 10. When investing in a system the user may be interested in deciding upfront which of the three configurations will provide the best economic solution. All systems are dimensioned to provide the peak shaving power even after 20 years, including capacity degradation. In addition, the restriction of a usable SOC range of RFB systems from 20% to 80% is considered [36]. The power electronics is dimensioned with 40 kW rated power. The Sony LFP cell technology for LIB and a scaled *CellDataStack5550W* model (cf. Table 4) as an all-Vanadium RFB system is considered. The assumed system costs for the economic evaluation are provided in Table D.11. As a revenue for reducing the power peak a fixed price of 100 EUR/kW in a yearly billing period is assumed. As an input power profile for the PS application, the Cluster 1 PS power profile from Kucevic et al. [73] is used and scaled to an annual load of 347.55 MWh from which the peak power is reduced to 63.5 kW.

After the simulation has been executed, the analysis and evaluation include both detailed technical and economic evaluations. An extract of the evaluations and results can be seen in the following illustrations:

Table 8
Matching of revenue streams and operation strategies for the cashflow calculation within the economic evaluation.

	ECR	DCR	FCR	SMT
Residential PV Greedy	x			
Residential PV Feed in Damp	x			
Peak Shaving	x	x		
Peak Shaving Perfect Foresight	x	x		
Frequency Containment Reserve			x	
Intraday Continuous Market				x

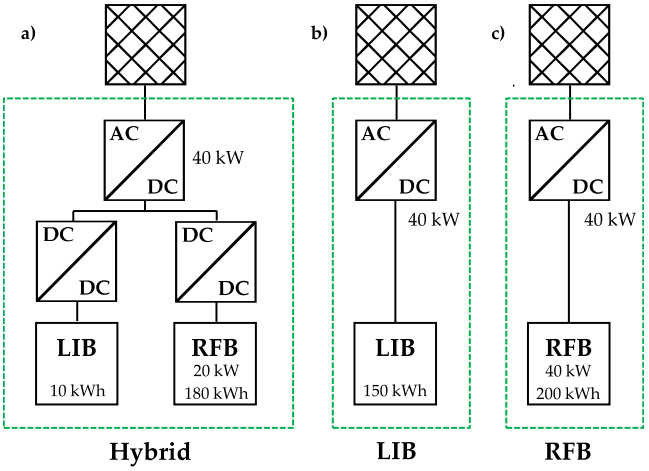

Fig. 10. Three different Energy Storage Systems (ESS) are investigated in the Peak Shaving (PS) case study: **(a)** A hybrid ESS consisting of a DC-coupled LIB and RFB system as well as single storage systems of **(b)** LIB and **(c)** RFB. All systems are dimensioned for providing the PS power even after 20 years of operation. A maximum Depth of Discharge (DOD) for RFB systems of 0.6 is considered. The Power Distribution Strategies (PDS) for the hybrid system performs according to the technology prioritization as described in Section 5.2.2. The DCDC converter is assumed with a fixed efficiency of 98%.

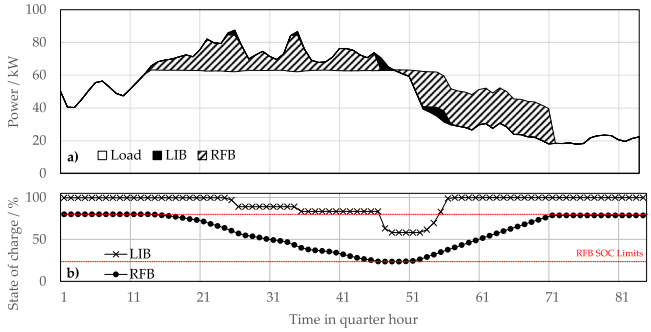

Fig. 11. Peak Shaving (PS) application on a hybrid Energy Storage System (ESS). **(a)** Residual load with and without the PS application with the delivered AC power of the installed ESS as well as the power distribution between the two DC-coupled storage systems. **(b)** State of Charge (SOC) development of the hybrid ESS. LIB systems takes over if target power exceed RFB stack power or if the RFB system hits its SOC limits.

Fig. 11 shows the characteristic curve of the power during the PS application for the hybrid storage system. The residual power can be seen with and without energy storage. It can be seen that the power drawn from the grid does not exceed the value of the PS threshold as was dictated by the operation strategy. Power demand values above the PS threshold are provided by the respective storage unit. This comes in line with charging and discharging power from the ESS and a simultaneous change in the storage-lumped SOC. According to the conditions set, recharging of the storage systems is executed only at times such that the PS threshold is never exceeded. In addition, the power distribution to the corresponding storage technologies of the hybrid system can be seen. The RFB system is prioritized to provide the bulk energy of the PS event while the LIB system covers high power peaks, especially if the RFB systems power capabilities are exhausted.

The remaining capacity (SOH) of the ESS can be seen in Fig. 12. The LIB capacity decreases to 70% during the 20-year simulation, while for the hybrid system as well as for the RFB system the capacity remains higher at 97% and 96%, respectively. Although the integrated degradation models consider both the calendar and the cycle degradation, it is noteworthy that the calendar degradation takes up the largest share in this operation of PS application [59].

In Fig. 12 the difference of the system round-trip efficiency can be observed. The LIB system demonstrates the highest efficiency with 88%, followed by the hybrid system with 68% and the RFB system with 62%. The energy losses of the RFB storage compartments are higher compared to LIB, attributed to a comparably low Coulomb efficiency and additional energy needed for electrolyte pumps.

In addition to the technical evaluation, **SimSES** also provides a comprehensive economic analysis of the simulated time series. In order to show a metric for overall costs, an alternative NPV considering capacity degradation as well is shown in Eq. (21), where c_{ST} represents energy-specific costs of the storage technology and C_{deg} the capacity degradation.

$$NPV_{CD} = NPV - c_{ST} \cdot C_{deg} \tag{21}$$

Fig. 12 shows the overall costs of the ESS operated with baseline cost set to 100% of the LIB system. For the evaluation of the system, not only real tariff models but also the investment costs for the ESS are integrated in the tool resulting in the NPV. In addition, the cost of capacity degradation is added to the NPV in order to take not only the system efficiency into account but also the capacity loss over 20 years (see Eq. (21)). It can be seen that the hybrid system is 5% more cost effective while the RFB system has 81% higher overall costs. The primary reason for these values are the cost of capacity degradation, which is 51% of the overall costs for the LIB system although the NPV for the LIB systems is lowest compared to the other systems. In conclusion, a hybrid system can deliver an overall better solution compared to single storage systems although only a small peak LIB ESS is added to an RFB system, combining the benefits of both techniques, i.e., a higher NPV compared to a single RFB system and a lower capacity degradation compared to a single LIB system. However, with the input parameters chosen herein, none of the three negative storage solutions were able to justify an investment as all resulted in negative NPV_{CD} values. The overall economics of this case study could potentially be improved if the ESS value generation was increased, e.g., by applying multi-use operation and dispatching storage in PS idle times [4,74]. Additionally, results with hybrid storage systems could be improved with optimization and machine learning techniques instead of applying a rule-based algorithm [75,76].

6.2. Case study 2: Frequency containment reserve application

A widely used application of utility-scale ESS is participation in the market for FCR. In this application, the ESS compensate for fluctuations

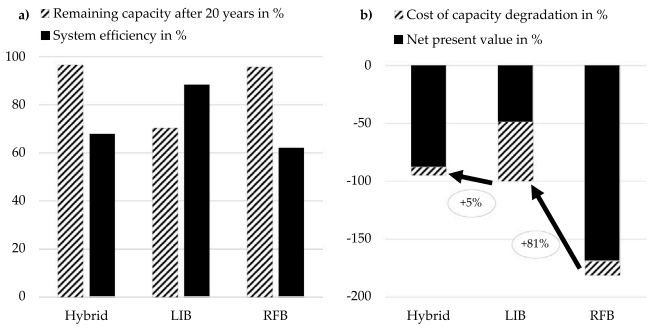

Fig. 12. Economic analysis of the three different Energy Storage Systems (ESS) serving the Peak Shaving (PS) application. **(a)** Comparison of remaining capacity and system efficiency of all simulated ESS after 20 years. **(b)** Overall costs consisting of the NPV and cost of capacity degradation using the LIB system as the baseline. The hybrid system could decrease overall cost by 5%, whereas the RFB system increased the cost by 81%.

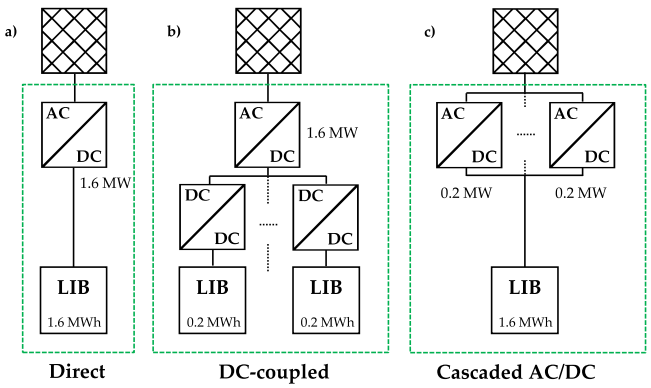

Fig. 13. Three different ESS topologies are investigated in the FCR case study, all with a LIB system of 1.6 MWh and an ACDC connection to the grid of 1.6 MW. The ACDC converter model is the *NottonAcDcConverter* (cf. Table 6). **(a)** A direct-coupled ESS with one ACDC converter. **(b)** Eight parallel DC-coupled systems with an assumed fixed DCDC efficiency of 98%. **(c)** Eight parallel connected ACDC converter with a cascaded activation: The first ACDC converter drives to its nominal power of 0.2 MW before the second ACDC converter is activated.

between consumption and generation in the power grid by reacting accordingly to changes in the grid frequency. The regulations and degrees of freedom for FCR application complying to German regulation criteria are taken into account and are described in detail in [4,8,62,73]. In this operation strategy of **SimSES** the SOC stabilization of the ESS is achieved by support of IDM. FCR and IDM are each basic operation strategies running in a stacked operation. For the simulation a grid frequency profile of 2014 is used to account for the provided stabilizing power [77]. It is assumed that the provided power of 1 MW does not affect the integrated network frequency.

In this case study, three different ESS topologies are simulated (cf. Fig. 13), each with a Sony LFP cell technology providing a capacity of 1.6 MWh and a grid-connection power of 1.6 MW. First, a simple direct approach of connecting a LIB to a grid-connected ACDC converter is investigated. Second, eight parallel DC-coupled systems with a LIB capacity of 0.2 MWh each are simulated. Third, eight parallel connected ACDC converters with a nominal power of 0.2 MW each are activated in a cascaded approach promising a higher efficiency [78]. The assumed system costs for the economic evaluation are provided in Table D.12. The revenue of FCR[12] is taken as a fixed price of 0.2 EUR per kW and day and the IDM[13] price is fixed to 0.04 EUR/kWh, corresponding to a price level of 2020.

The results of the 20-year simulations are displayed in Fig. 14. The cascaded ACDC converter approach shows the best efficiency with 92% compared to the direct approach with 78% and the least efficient topology with DC-coupled systems of 63%. FCR is an application with a high partial-load frequency below 30% of nominal power [55]. Hence, the cascaded ACDC converter are either under a high load compared to their nominal power or deactivated, leading to a higher overall efficiency compared to the direct system. The DC-coupled system shows an overproportional efficiency decrease compared to the direct system. The systems of the DC-coupled ESS are activated similar to the cascade of ACDC converter: one system is ramped up to full power before the second system is activated. Due to relatively high currents in addition to the losses of the DCDC converter, the DC-coupled system shows a comparatively low efficiency. This result suggests that the chosen PDS is inappropriate in terms of efficiency for a FCR application with the given system for the DC-coupled system. Comparing the remaining capacity of the three investigated systems, no large difference can be observed, with a remaining capacity of each system after 20 years of around 80%. One target of the chosen PDS for the DC-coupled system was to reduce the capacity degradation by cycling a few systems more often than other systems in order to get an overall better degradation behavior. However, it can be observed that the chosen strategy shows no improvement in terms of the degradation behavior for this application compared to the other systems.

Analyzing the economics, the high efficiency advantage of the cascaded system could be transferred to a slight monetary improvement compared to the other systems. The cascaded system shows a 4% increase of the NPV compared to the direct system. The DC-coupled system falls behind with a lower NPV of 5% in comparison to the direct system (cf. Fig. 14). This could be explained with IDM recharging cost over the simulation time period since the FCR revenue is the same for all investigated systems (cf. Table 9).

First, the IDM transaction costs are comparatively low: The direct system accounts for 36 kEUR, the DC-coupled system for 64 kEUR and the cascaded system for 14 kEUR, accumulated after 20 years of operation. In comparison, the FCR revenue compensates for around 1,218 kEUR. Second, the low efficiency of the DC-coupled system results in 231 MWh energy sold on the IDM whereas the direct system and the cascaded system could sell 347 MWh and 494 MWh, respectively. This is also reflected in the numbers of bought energy: the DC-coupled system had to buy most energy with 1,829 MWh while the cascaded system had to buy 851 MWh. Although large differences in terms of efficiency exist compared to the direct system (+14% for the cascaded system and -15% for the DC-coupled system) this could only be translated into a 4% increase of the NPV, respectively to a 5% decrease. The economic result of more efficient ESS could be improved by reducing the storage capacity and improving the IDM operation strategy. In conclusion, all three systems have a positive NPV, likely leading to a positive investment decision.

With these case studies a high variety of topologies as well as technology combinations could be investigated. Parameter variations, e.g., for the investment costs or sizing of individual components can easily be made by the user when adapting according initialization files of the case studies available as presented in Appendix E.

7. Conclusion and outlook

Within this work, the simulation and analysis tool for energy storage systems **SimSES** is presented. **SimSES** provides a library of state-of-the-art energy storage models by combining modularity of multiple topologies as well as the periphery of an ESS. This paper summarizes the structure as well as the capabilities of **SimSES**. Storage technology

[12] Prices for the German FCR market can be found at https://www.regelleistung.net.

[13] Prices for the European spot market can be found at https://www.epexspot.com.

Table 9
Overview of the IDM transaction costs for all three investigated ESS.

System	IDM transaction costs/EUR	Energy bought/MWh	Energy sold/MWh
Direct	35,772	1242	347
DC-coupled	63,894	1829	231
Cascaded	14,280	851	494

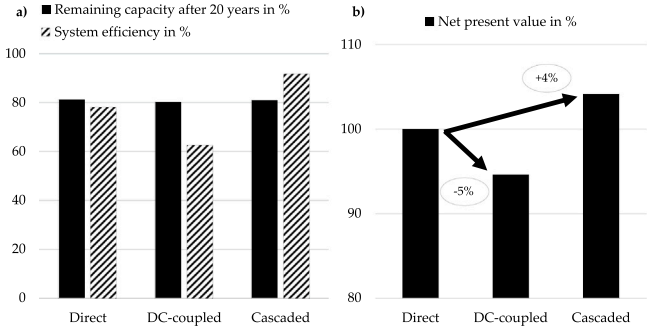

Fig. 14. Technical and economical analysis of the three different Energy Storage Systems (ESS) serving the Frequency Containment Reserve (FCR) application. **(a)** Comparison of remaining capacity after 20 years and system efficiency of all simulated ESSs. **(b)** Economic value consisting of the NPV using the direct system as baseline.

models based on current research for lithium-ion batteries, redox flow batteries, as well as hydrogen storage-based electrolysis and fuel cell are presented in detail. In addition, thermal models and their corresponding HVAC systems, housing, and ambient models are depicted. Power electronics are represented with ACDC and DCDC converters mapping the main losses of power electronics within a storage system. Additionally, auxiliary components like pumps, compressors, and HVAC are considered. Standard use cases like peak shaving, residential storage, and control reserve power provisions through dispatch of storage are discussed in this work, with the possibility to stack these applications in a multi-use scenario. The analysis is provided by technical and economic evaluations illustrated by KPIs.

SimSES' capabilities are demonstrated through the discussion of two case studies mapped to the applications of peak shaving and frequency containment reserve, respectively. It is demonstrated how different energy storage system topologies as well as various performance indicators can be investigated and analyzed with **SimSES**. For the specific cases discussed, the results underline that hybrid storage systems can lead in terms of overall cost and degradation behavior to a beneficial economic results. Special ESS topologies like the cascaded ACDC converter approach can lead to a substantial increase in system efficiency for the FCR application, although the economic benefits are comparatively low.

In the future, more detailed performance and aging models for all types of storage systems will be implemented. This will allow a more detailed cross-technology comparison. For instance, models for bidirectional thermal storage system could be implemented in future versions. Further operating strategies matching internationally renowned and national derivatives of application scenarios could also be investigated. This may allow assessing the value of storage deployment across different regions and convince internationally active investors to reveal best investment scenarios worldwide. **SimSES** has interfaces that can be easily integrated into physically derived and more accurate storage models as well as grid modeling and system analysis tools. While selected validation experiments have already been executed, the authors encourage others in the research community to conduct hardware validation experiments at their sites and contribute to the presented tool. The authors envision interlinking **SimSES** to the vast selection of open-source tools in order to expand on the value chain that storage simulations are capable of covering, e.g., **SimSES** is already a part of the *openMOD*[14] initiative. **SimSES** is open-source available, and the authors encourage users and developers to join in and assist in its further development.

CRediT authorship contribution statement

Marc Möller: Conceptualization, Methodology, Writing - original draft, Writing - review & editing, Software, Project administration, Visualization, Investigation. **Daniel Kucevic:** Writing - original draft, Writing - review & editing, Validation, Software, Methodology. **Nils Collath:** Writing - original draft, Writing - review & editing, Software, Methodology. **Anupam Parlikar:** Writing - original draft, Writing - review & editing, Software, Methodology. **Petra Dotzauer:** Writing - original draft, Writing - review & editing, Software, Methodology. **Benedikt Tepe:** Investigation, Validation, Writing - original draft, Writing - review & editing, Software. **Stefan Englberger:** Investigation, Validation, Writing - original draft, Writing - review & editing. **Andreas Jossen:** Writing - review & editing, Funding acquisition. **Holger Hesse:** Writing - original draft, Writing - review & editing, Supervision.

Declaration of competing interest

The authors declare that they have no known competing financial interests or personal relationships that could have appeared to influence the work reported in this paper.

Acknowledgments

This work was financially supported by the Federal Ministry for Economic Affairs and Energy within the open_BEA project (Grant No. 03ET4072) and the EffSkalBatt project (Grant No. 03ET6148). Both projects are supported by Project Management Juelich. The responsibility for this publication rests with the authors.

We thank Jacob Klinkenberg, Kareem Abo Gamra, and Benedikt Wiesend for their contribution with simulating and implementing models in the hydrogen package, Timo Sandner and Felix Müller for their implementations of ACDC converters, Dang The Phong for his work on the model for a RFB stack as well as Ni Chuanqin and Yuhui Geng for their implementations of two LIB degradation models.

Appendix A. Open circuit voltage curve fitting

The OCV for LIBs (see Section 4.1) is dependent on the cell type. The OCV data for all currently implemented cell types have been measured at the Institute for Electrical Energy Storage Technology at the Technical University of Munich. To improve the performance, the look-up tables of the voltage values are replaced with a mathematical function. These curve-fitting functions are based on the work of Weng et al. [79]. The parameters of this function for the OCV are estimated using the MATLAB® global optimization toolbox. Fig. A.15 shows the OCV in V for the measured data as well as the curve-fitted data and the difference between those in mV.

[14] https://openmod-initiative.org/

Table B.10
Physical parameters for modeling of thermal behavior of lithium-ion batteries (LIBs).

Manufacturer model	Mass (g)	Dimensions (mm)	Specific heat ($Jkg^{-1}K^{-1}$)	Convection coefficient ($Wm^{-2}K^{-1}$)	Source
Sony US26650FTC1	70	dia: 26 len: 65	1001	15	[55,80–89]
Panasonic NCR18650PD	44	dia: 18 len: 65	1048	15	[88–90]
E-One Moli Energy IHR18650A	45	dia: 18 len: 65	965	15	[83,86,89,91–94]
Sanyo UR18650E	46	dia: 18 len: 65	965	15	[83,86,89,92–95]

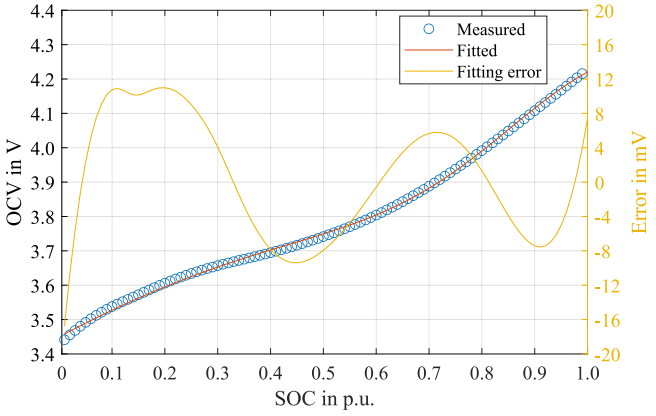

Fig. A.15. Open Circuit Voltage (OCV) curve fitting for the MolicelNMC lithium-ion battery (LIB). The figure shows the OCV in V for the measured data as well as the curve-fitted data and the difference between those in mV.

Appendix B. Thermal parameters

The geometrical and thermal parameters used for modeling the thermal behavior of LIBs are presented in Table B.10. Geometrical parameters such as the dimensions and the weight are obtained from datasheets of the cells. The thermal properties, such as the specific heat capacity for each cell type, are determined from the literature for each cell chemistry, and averaged over several values found in the literature. The value of the convection coefficient is known with the least accuracy, and a value of 15 $Wm^{-2}K^{-1}$ is selected as a "reasonable" value lying between typical values for purely natural convection and forced convection. This is assumed to emulate slow intermittent motion of air around the cells. It is expected that availability of better data in the future will increase the accuracy of the modeling process.

Appendix C. Stack data for a redox flow battery

The parameters are based on single-cell measurements carried out at ZAE Bayern of a cell with a technical representative cell area of 2160 cm^2. To obtain parameters for a stack, the measured values were scaled up with a number of 40 cells. Fig. C.16 shows the data of the internal resistance of the 40-cell stack for charge and discharge. The internal resistance is determined by applying a constant current and measuring the resulting change of voltage. The cell was operating in Vanadium electrolyte (1.6 mol/l V solved in 2 mol/l H_2SO_4) from GfE (Gesellschaft für Elektrometallurgie mbH). Temperature and flow rate were controlled during the procedure. The SOC was determined with an OCV-cell. Due to the relatively high ohmic resistance of the cell and the low possible operation current density (up to approx. 50 mA/cm^2), the cell resistance shows no significant current dependency. The cell

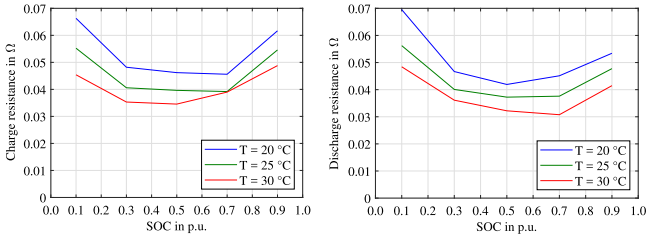

Fig. C.16. Charge and discharge resistance of a stack for a redox flow battery (cell area = 2160 cm^2) dependent on State of Charge (SOC) and temperature (T). The single-cell measurements were scaled up to a stack resistance with a cell number of 40.

resistance R_{cell} was scaled up with the number of cells n_{cell} to receive the stack resistance R_{stack} ($R_{stack} = n_{cell} \cdot R_{cell}$).

Appendix D. Economics for case studies

Assumptions for economical analysis of the case studies are based on Tsiropoulos et al. Minke et al. Figgener et al. and Mongird et al. [96–99]. Challenges for determining energy-specific costs for ESS occur due to a wide range of technology costs as well as various system sizes and designs. In order to distinguish between power and energy system design, Tsiropoulos et al. takes the EPR as an indicator: If EPR is above one, the authors talk about an energy-driven design, otherwise about power-driven design [96]. In addition, it is not always clearly stated which costs for a system design are included, e.g., power electronics, housing, and grid connection [96,98]. For instance, utility scale system costs for LIB in 2017 ranged between 300 EUR/kWh and 1200 EUR/kWh with an average around 570 EUR/kWh [96]. Figgener et al. depicted a similar range for 2018 [98] as well as one reported system for 2019 with an EPR of 1 h and system costs of around 900 EUR/kWh. However, LIB systems with an EPR of 0.125 h show lowest cost with 300 EUR/kWh and costs increase with rising EPR [96]. Mongird et al. have presented system costs for LIB system with an EPR larger than 1 h with falling costs [99]. Interestingly, the system costs of [99] show a lower average system cost price than those of [96,98] representing European costs' levels (a USD to EUR conversion of 0.82 is assumed). In contrast, a broad cost database does not exist for RFB systems. However, Minke et al. investigated various RFB projects from 2004 to 2017 by determining system prices for different EPR, similar to Tsiropoulos et al. [97]. The authors also found an even broader range of system costs for RFB from 155 EUR/kWh to 1738 EUR/kWh, especially due to different electrolytes, stack modules, sizing, and system definition. RFB system costs decrease with a rising EPR with average system costs of 717 EUR/kWh for an EPR of 2 h and 166 EUR/kWh for a ratio of 15 h. These findings are also in agreement with the results of Mongird et al. [99].

For the following case studies, system cost curves depending on EPR are assumed for LIB and RFB systems with the prices and ratios

Table D.11
Economics for Case Study 1.

Storage technology	Power/kW	Capacity/kWh	EPR/h	Specific system cost/EUR kWh^{-1}	System cost/EUR	Overall system cost/EUR
LIB	40	10	0.25	584	5,839	
RFB	20	180	9.00	329	59,216	65,055
LIB only	40	150	3.75	367	55,089	55,089
RFB only	40	200	5.00	451	90,247	90,247

Table D.12
Economics for Case Study 2.

Storage technology	Power/kW	Capacity/kWh	EPR/h	Specific system cost/EUR kWh^{-1}	System cost/EUR
LIB	1,600	1,600	1	473	756,800

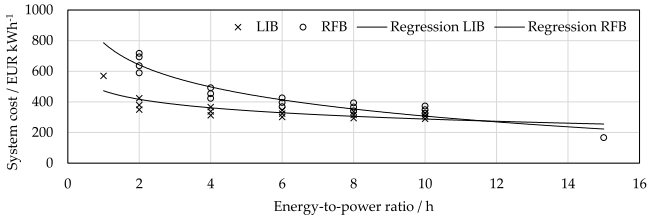

Fig. D.17. System costs curves depending on EPR for LIB and RFB systems based on [96,97,99].

given represented by regression curves in Eqs. (D.1) and (D.2). From an EPR of 1 h up to 15 h, this cost curve has a realistic cost range with decreasing cost over EPR. The system costs, however, have a high uncertainty attached, as shown in the previous analysis. The used price curves are shown in Fig. D.17. It is worth mentioning that the cost assumptions for RFB systems are based on a usable SOC range of 20% and 80%, which reduces the gross capacity configured by 40% [97].

$$c_{LIB} = -80 \cdot \ln(EPR) + 473 \quad \text{and} \tag{D.1}$$

$$c_{RFB} = -208 \cdot \ln(EPR) + 786, \tag{D.2}$$

where c represents the energy specific costs of LIB, respectively RFB.

Using Eqs. (D.1) and (D.2) the system costs for the two case studies discussed in Section 6 are calculated as provided in Tables D.11 and D.12.

Appendix E. Availability of SimSES

SimSES is available as open source[15] and is part of the open-source simulation and optimization toolchain of the Institute for Electrical Energy Storage Technology at the Technical University of Munich.[16] A *readme.md* helps with the first steps in order to get **SimSES** running. An installed Python environment is mandatory as well as the required packages installed automatically if you run *setup.py*. With executing *main.py*, a default configured simulation could be started directly. This file offers also all necessary interfaces in order to connect it to other simulation programs. The case studies presented within this paper are conducted with the open-source release version 1.0.4.

For configuring a simulation, there are two important configuration files: *simulation.ini* and *analysis.ini*. These configuration files are documented and offer all possible settings for setting up a simulation and the consequent evaluation. These config files follow a pattern for a *default* and *local* configuration. The *default* configuration inherits all possible settings, in the *local* file: only the changed settings are necessary. This allows a quick exchange of configuration settings between users.

The *Simulation* package allows multiple simultaneous simulations, which are also used for the presented case studies. In here, the configurations and code could be found with the case study configs in *case_studies*. In order to execute the case studies, the configuration needs to be copied to the config location and renamed to *simulation.local.ini*.

[15] https://gitlab.lrz.de/open-ees-ses/simses
[16] http://www.simses.org

References

[1] V. Lauber, S. Jacobsson, The politics and economics of constructing, contesting and restricting socio-political space for renewables – the German renewable energy act, Environ. Innov. Soc. Transitions 18 (2016) 147–163, http://dx.doi.org/10.1016/j.eist.2015.06.005.
[2] H.E. Murdock, D. Gibb, T. André, F. Appavou, A. Brown, B. Epp, B. Kondev, A. McCrone, E. Musolino, L. Ranalder, Renewables 2019 global status report, REN21, https://www.ren21.net/wp-content/uploads/2019/05/gsr_2019_full_report_en.pdf.
[3] P. Denholm, E. Ela, B. Kirby, M. Milligan, The Role of Energy Storage with Renewable Electricity Generation, Technical Report NREL (2010), 2010, http://dx.doi.org/10.2172/972169.
[4] S. Englberger, A. Jossen, H. Hesse, Unlocking the potential of battery storage with the dynamic stacking of multiple applications, Cell Rep. Phys. Sci. 1 (11) (2020) http://dx.doi.org/10.1016/j.xcrp.2020.100238.
[5] A. Evans, V. Strezov, T.J. Evans, Assessment of utility energy storage options for increased renewable energy penetration, Renew. Sustain. Energy Rev. 16 (6) (2012) 4141–4147, http://dx.doi.org/10.1016/j.rser.2012.03.048.
[6] D. Zafirakis, K.J. Chalvatzis, G. Baiocchi, G. Daskalakis, The value of arbitrage for energy storage: Evidence from European electricity markets, Appl. Energy 184 (2016) 971–986, http://dx.doi.org/10.1016/j.apenergy.2016.05.047.
[7] R.H. Byrne, R.J. Concepcion, C.A. Silva-Monroy, Estimating potential revenue from electrical energy storage in PJM, in: IEEE Power and Energy Society General Meeting (2016), 2016, http://dx.doi.org/10.1109/PESGM.2016.7741915.
[8] T. Thien, D. Schweer, D. vom Stein, A. Moser, D.U. Sauer, Real-world operating strategy and sensitivity analysis of frequency containment reserve provision with battery energy storage systems in the german market, J. Energy Storage 13 (2017) 143–163, http://dx.doi.org/10.1016/j.est.2017.06.012.
[9] A. Oudalov, R. Cherkaoui, Sizing and optimal operation of battery energy storage system for peak shaving application: Lausanne, Switzerland, 1 - 5 july 2007, IEEE Lausanne Power Tech. (2007) http://dx.doi.org/10.1109/PCT.2007.4538388.
[10] J. Hoppmann, J. Volland, T.S. Schmidt, V.H. Hoffmann, The economic viability of battery storage for residential solar photovoltaic systems – A review and a simulation model, Renew. Sustain. Energy Rev. 39 (2014) 1101–1118, http://dx.doi.org/10.1016/j.rser.2014.07.068.
[11] H. Hesse, R. Martins, P. Musilek, M. Naumann, C. Truong, A. Jossen, Economic optimization of component sizing for residential battery storage systems, Energies 10 (7) (2017) 835, http://dx.doi.org/10.3390/en10070835.
[12] S. Englberger, H. Hesse, D. Kucevic, A. Jossen, A techno-economic analysis of vehicle-to-building: Battery degradation and efficiency analysis in the context of coordinated electric vehicle charging, Energies 12 (5) (2019) 955, http://dx.doi.org/10.3390/en12050955.
[13] O.M. Toledo, D. Oliveira Filho, A.S.A.C. Diniz, Distributed photovoltaic generation and energy storage systems: A review, Renew. Sustain. Energy Rev. 14 (1) (2010) 506–511, http://dx.doi.org/10.1016/j.rser.2009.08.007.
[14] H. Hesse, M. Schimpe, D. Kucevic, A. Jossen, Lithium-ion battery storage for the grid—A review of stationary battery storage system design tailored for applications in modern power grids, Energies 10 (12) (2017) 2107, http://dx.doi.org/10.3390/en10122107.
[15] B. Dunn, H. Kamath, J.-M. Tarascon, Electrical energy storage for the grid: A battery of choices, Science 334 (2011) http://dx.doi.org/10.1126/science.1212741.

[16] J. Weniger, T. Tjaden, Performance-Simulationsmodell für AC-gekoppelte PV-Batteriesysteme (PerModAC): Dokumentation | Version 1.0, Hochschule für Technik und Wirtschaft H.T.W. Berlin, Berlin, 2017, URL https://pvspeicher.htw-berlin.de/wp-content/uploads/2017/03/PerModAC_doku.pdf.

[17] N.-K.C. Nair, N. Garimella, Battery energy storage systems: Assessment for small-scale renewable energy integration, Energy Build. 42 (11) (2010) 2124–2130, http://dx.doi.org/10.1016/j.enbuild.2010.07.002.

[18] U. Sureshkumar, P.S. Manoharan, A.P.S. Ramalakshmi, Economic cost analysis of hybrid renewable energy system using HOMER, in: IEEE-International Conference on Advances in Engineering, Science and Management, ICAESM -2012, 2012, pp. 94–99.

[19] J. Figgener, P. Stenzel, K.-P. Kairies, J. Linßen, D. Haberschusz, O. Wessels, G. Angenendt, M. Robinius, D. Stolten, D.U. Sauer, The development of stationary battery storage systems in Germany – A market review, J. Energy Storage 29 (2020) http://dx.doi.org/10.1016/j.est.2019.101153.

[20] E. Gamma, R. Helm, R. Johnson, J.M. Vlissides, Design Patterns: Elements of Reusable Object-Oriented Software, first ed., Addison-Wesley Professional, 1994.

[21] B. Nykvist, M. Nilsson, Rapidly falling costs of battery packs for electric vehicles, Nature Clim. Change 5 (4) (2015) 329–332, http://dx.doi.org/10.1038/nclimate2564.

[22] G. Zubi, R. Dufo-López, M. Carvalho, G. Pasaoglu, The lithium-ion battery: State of the art and future perspectives, Renew. Sustain. Energy Rev. 89 (2018) 292–308, http://dx.doi.org/10.1016/j.rser.2018.03.002.

[23] M. Yoshio, R.J. Brodd, A. Kozawa, Lithium-Ion Batteries, Springer New York, New York, NY, 2009, http://dx.doi.org/10.1007/978-0-387-34445-4.

[24] A.M. Divakaran, M. Minakshi, P.A. Bahri, S. Paul, P. Kumari, A.M. Divakaran, K.N. Manjunatha, Rational design on materials for developing next generation lithium-ion secondary battery, Prog. Solid State Chem. 62 (2021) 100298, http://dx.doi.org/10.1016/j.progsolidstchem.2020.100298.

[25] M. Naumann, F.B. Spingler, A. Jossen, Analysis and modeling of cycle aging of a commercial LiFePO4/graphite cell, J. Power Sources 451 (2020) 227666, http://dx.doi.org/10.1016/j.jpowsour.2019.227666.

[26] M. Naumann, M. Schimpe, P. Keil, H.C. Hesse, A. Jossen, Analysis and modeling of calendar aging of a commercial LiFePO4/graphite cell, J. Energy Storage 17 (2018) 153–169, http://dx.doi.org/10.1016/j.est.2018.01.019.

[27] P. Keil, S.F. Schuster, J. Wilhelm, J. Travi, A. Hauser, R.C. Karl, A. Jossen, Calendar aging of lithium-ion batteries, J. Electrochem. Soc. 163 (9) (2016) A1872–A1880, http://dx.doi.org/10.1149/2.0411609jes.

[28] S.F. Schuster, T. Bach, E. Fleder, J. Müller, M. Brand, G. Sextl, A. Jossen, Nonlinear aging characteristics of lithium-ion cells under different operational conditions, J. Energy Storage 1 (2015) 44–53, http://dx.doi.org/10.1016/j.est.2015.05.003.

[29] J. Schmalstieg, S. Käbitz, M. Ecker, D.U. Sauer, A holistic aging model for li(NiMnCo)o2 based 18650 lithium-ion batteries, J. Power Sources 257 (2014) 325–334, http://dx.doi.org/10.1016/j.jpowsour.2014.02.012.

[30] M.M. Rahman, A.O. Oni, E. Gemechu, A. Kumar, Assessment of energy storage technologies: A review, Energy Convers. Manage. 223 (2020) 113295, http://dx.doi.org/10.1016/j.enconman.2020.113295.

[31] G. Kear, A.A. Shah, F.C. Walsh, Development of the all-vanadium redox flow battery for energy storage: a review of technological, financial and policy aspects, Int. J. Energy Res. 36 (11) (2012) 1105–1120, http://dx.doi.org/10.1002/er.1863.

[32] A.Z. Weber, M.M. Mench, J.P. Meyers, P.N. Ross, J.T. Gostick, Q. Liu, Redox flow batteries: a review, J. Appl. Electrochem. 41 (10) (2011) 1137–1164, http://dx.doi.org/10.1007/s10800-011-0348-2.

[33] N. Hagedorn, M.A. Hoberecht, L.H. Thaller, NASA redox cell stack shunt current, pumping power, and cell performance tradeoffs, U.S. Department of Energy / NASA Technical Memorandum, 1982, URL https://ntrs.nasa.gov/citations/19820011459.

[34] R. Schweiss, A. Pritzl, C. Meiser, Parasitic hydrogen evolution at different carbon fiber electrodes in vanadium redox flow batteries, J. Electrochem. Soc. 163 (9) (2016) A2089–A2094, http://dx.doi.org/10.1149/2.1281609jes.

[35] A.H. Whitehead, M. Harrer, Investigation of a method to hinder charge imbalance in the vanadium redox flow battery, J. Power Sources 230 (2013) 271–276, http://dx.doi.org/10.1016/j.jpowsour.2012.11.148.

[36] M. Skyllas-Kazacos, L. Cao, M. Kazacos, N. Kausar, A. Mousa, Vanadium electrolyte studies for the vanadium redox battery-a review, ChemSusChem 9 (13) (2016) 1521–1543, http://dx.doi.org/10.1002/cssc.201600102.

[37] A. Tang, J. Bao, M. Skyllas-Kazacos, Studies on pressure losses and flow rate optimization in vanadium redox flow battery, J. Power Sources 248 (2014) 154–162, http://dx.doi.org/10.1016/j.jpowsour.2013.09.071.

[38] E.A. Kaminski, R.F. Savinell, A technique for calculating shunt leakage and cell currents in bipolar stacks having divided or undivided cells, J. Electrochem. Soc. 130 (5) (1983) 1103–1107.

[39] fumatech, in: fumatech (Ed.), Redox-Flow-Batteries: data sheet: fumasep® membrane types, URL https://www.fumatech.com/NR/rdonlyres/6E4FA7B9-0AAA-42B9-98E4-BF756C23F981/0/FUMATECH_BWT_GmbHRedoxFlowBatteries.pdf.

[40] C. Blanc, R. Alfred, Understanding the vanadium redox flow batteries, in: InTech (Ed.), Paths to Sustainable Energy, InTechOpen, 2010, pp. 333–358.

[41] M. Robinius, P. Markewitz, P. Lopion, D. Stolten, Cost-efficient and climate-friendly transformation strategies for the german energy system up to 2050, in: Forschungszentrum JÜLich: Energy & Environment, 499, 2019.

[42] R.P. O'Hayre, S.-W. Cha, W.G. Colella, F.B. Prinz, Fuel cell fundamentals, third ed., John Wiley & Sons Inc, Hoboken New Jersey, 2016.

[43] G. Tjarks, PEM-electrolysis-systems for the integration in power-to-gas applications, (Ph.D. thesis), Lehrstuhl für Brennstoffzellen, RWTH Aachen, Aachen, 2017, http://dx.doi.org/10.18154/RWTH-2017-04470.

[44] C. Rakousky, U. Reimer, K. Wippermann, M. Carmo, W. Lueke, D. Stolten, An analysis of degradation phenomena in polymer electrolyte membrane water electrolysis, J. Power Sources 326 (2016) 120–128, http://dx.doi.org/10.1016/j.jpowsour.2016.06.082.

[45] C. Rakousky, U. Reimer, K. Wippermann, S. Kuhri, M. Carmo, W. Lueke, D. Stolten, Polymer electrolyte membrane water electrolysis: Restraining degradation in the presence of fluctuating power, J. Power Sources 342 (2017) 38–47, http://dx.doi.org/10.1016/j.jpowsour.2016.11.118.

[46] F. Marangio, M. Santarelli, M. Cali, Theoretical model and experimental analysis of a high pressure pem water electrolyser for hydrogen production, Int. J. Hydrogen Energy 34 (3) (2009) 1143–1158, http://dx.doi.org/10.1016/j.ijhydene.2008.11.083.

[47] M. Hammoudi, C. Henao, K. Agbossou, Y. Dubé, M.L. Doumbia, New multi-physics approach for modelling and design of alkaline electrolyzers, Int. J. Hydrogen Energy 37 (19) (2012) 13895–13913, http://dx.doi.org/10.1016/j.ijhydene.2012.07.015.

[48] C. Henao, K. Agbossou, M. Hammoudi, Y. Dubé, A. Cardenas, Simulation tool based on a physics model and an electrical analogy for an alkaline electrolyser, J. Power Sources 250 (2014) 58–67, http://dx.doi.org/10.1016/j.jpowsour.2013.10.086.

[49] D. Feroldi, M.S. Basualdo, Description of PEM Fuel Cells Systems, Springer, London and New York, 2012, http://dx.doi.org/10.1007/978-1-84996-184-4_2.

[50] A. Buttler, H. Spliethoff, Current status of water electrolysis for energy storage, grid balancing and sector coupling via power-to-gas and power-to-liquids: A review, Renew. Sustain. Energy Rev. 82 (2018) 2440–2454, http://dx.doi.org/10.1016/j.rser.2017.09.003.

[51] Q. Feng, X.-Z. Yuan, G. Liu, B. Wei, Z. Zhang, H. Li, H. Wang, A review of proton exchange membrane water electrolysis on degradation mechanisms and mitigation strategies, J. Power Sources 366 (2017) 33–55, http://dx.doi.org/10.1016/j.jpowsour.2017.09.006.

[52] A. Ursúa, E.L. Barrios, J. Pascual, I. San Martín, P. Sanchis, Integration of commercial alkaline water electrolysers with renewable energies: Limitations and improvements, Int. J. Hydrogen Energy 41 (30) (2016) 12852–12861, http://dx.doi.org/10.1016/j.ijhydene.2016.06.071.

[53] M. Schimpe, N. Becker, T. Lahlou, H.C. Hesse, H.-G. Herzog, A. Jossen, Energy efficiency evaluation of grid connection scenarios for stationary battery energy storage systems, Energy Procedia 155 (2018) 77–101, http://dx.doi.org/10.1016/j.egypro.2018.11.065.

[54] G. Notton, V. Lazarov, L. Stoyanov, Optimal sizing of a grid-connected PV system for various PV module technologies and inclinations, inverter efficiency characteristics and locations, Renew. Energy 35 (2) (2010) 541–554, http://dx.doi.org/10.1016/j.renene.2009.07.013.

[55] M. Schimpe, M. Naumann, N. Truong, H.C. Hesse, S. Santhanagopalan, A. Saxon, A. Jossen, Energy efficiency evaluation of a stationary lithium-ion battery container storage system via electro-thermal modeling and detailed component analysis, Appl. Energy 210 (2018) 211–229, http://dx.doi.org/10.1016/j.apenergy.2017.10.129.

[56] M. Förstl, N. Truon, M. Möller, H. Hesse, A. Singer, T. Weyh, The efficiency and profitability of the modular multilevel battery for frequency containment reserve, Atlantis Highlights Eng. 6 (2020) 80–85, http://dx.doi.org/10.2991/ahe.k.210202.012.

[57] A. Zeh, R. Witzmann, Operational strategies for battery storage systems in low-voltage distribution grids to limit the feed-in power of roof-mounted solar power systems, Energy Procedia 46 (2014) 114–123, http://dx.doi.org/10.1016/j.egypro.2014.01.164.

[58] D. Kucevic, C.N. Truong, A. Jossen, H.C. Hesse, Lithium-ion battery storage design for buffering fast charging stations for battery electric vehicles and electric buses, in: D. Schulz (Ed.), NEIS 2018, VDE VERLAG GMBH, Berlin, 2019, pp. 1–6, URL http://ieeexplore.ieee.org/stamp/stamp.jsp?tp=&arnumber=8669466&isnumber=8669446.

[59] N. Collath, S. Englberger, A. Jossen, H. Hesse, Reduction of battery energy storage degradation in peak shaving operation through load forecast dependent energy management, in: D. Schulz (Ed.), NEIS 2020, VDE VERLAG GMBH, 2020, pp. 250–254, URL https://ieeexplore.ieee.org/stamp/stamp.jsp?tp=&arnumber=9273426.

[60] D. Übertragungsnetzbetreiber, Eckpunkte und Freiheitsgrade bei Erbringung von Primaerregelleistung (in German): Leitfaden für Anbieter von Primaerregelleistung, Berlin, Germany, 50Hertz Transmission GmbH and Amprion GmbH and TenneT TSO GmbH and TransnetBW GmbH, https://www.regelleistung.net/ext/download/eckpunktePRL.

[61] D. Übertragungsnetzbetreiber, Anforderungen an die Speicherkapazitaet bei Batterien für die Primaerregelleistung (in German), Berlin, Germany, 50Hertz Transmission GmbH and Amprion GmbH and TenneT TSO GmbH and TransnetBW GmbH, https://www.bves.de/wp-content/uploads/2015/08/2015_08_26_Anforderungen_Speicherkapazitaet_Batterien_PRL.pdf.

[62] A. Zeh, M. Müller, M. Naumann, H. Hesse, A. Jossen, R. Witzmann, Fundamentals of using battery energy storage systems to provide primary control reserves in Germany, Batteries 2 (3) (2016) 29, http://dx.doi.org/10.3390/batteries2030029.

[63] M. Mühlbauer, O. Bohlen, M.A. Danzer, Analysis of power flow control strategies in heterogeneous battery energy storage systems, J. Energy Storage 30 (2020) 101415, http://dx.doi.org/10.1016/j.est.2020.101415.

[64] M. Bauer, System Design and Power Flow of Stationary Energy Storage Systems, (Ph.D. thesis), ETH Zurich, 2019, http://dx.doi.org/10.3929/ETHZ-B-000374736.

[65] C.N. Truong, M. Naumann, R.C. Karl, M. Müller, A. Jossen, H.C. Hesse, Economics of residential photovoltaic battery systems in Germany: The case of teslas powerwall, Batteries 2 (2) (2016) 14, http://dx.doi.org/10.3390/batteries2020014.

[66] A.M. Divakaran, D. Hamilton, K.N. Manjunatha, M. Minakshi, Design, development and thermal analysis of reusable li-ion battery module for future mobile and stationary applications, Energies 13 (6) (2020) 1477, http://dx.doi.org/10.3390/en13061477.

[67] D. Wang, Y. Bao, J. Shi, Online lithium-ion battery internal resistance measurement application in state-of-charge estimation using the extended Kalman filter, Energies 10 (9) (2017) 1284, http://dx.doi.org/10.3390/en10091284.

[68] C.R. Birkl, M.R. Roberts, E. McTurk, P.G. Bruce, D.A. Howey, Degradation diagnostics for lithium ion cells, J. Power Sources 341 (2017) 373–386, http://dx.doi.org/10.1016/j.jpowsour.2016.12.011.

[69] T. Waldmann, M. Wilka, M. Kasper, M. Fleischhammer, M. Wohlfahrt-Mehrens, Temperature dependent ageing mechanisms in lithium-ion batteries – a post-mortem study, J. Power Sources 262 (2014) 129–135, http://dx.doi.org/10.1016/j.jpowsour.2014.03.112.

[70] S. Ma, M. Jiang, P. Tao, C. Song, J. Wu, J. Wang, T. Deng, W. Shang, Temperature effect and thermal impact in lithium-ion batteries: A review, Prog. Nat. Sci. Mater. Int. 28 (6) (2018) 653–666, http://dx.doi.org/10.1016/j.pnsc.2018.11.002.

[71] B. Shabani, M. Biju, Theoretical modelling methods for thermal management of batteries, Energies 8 (9) (2015) 10153–10177, http://dx.doi.org/10.3390/en80910153.

[72] Deutsches Zentrum für Luft- und Raumfahrt (DLR) / German Aerospace Centre, greenius: Green Energy System Analysis, Deutsches Zentrum für Luft- und Raumfahrt (DLR) / German Aerospace Centre, Köln, Germany, 2018, URL https://www.dlr.de/sf/en/desktopdefault.aspx/tabid-11688/20442_read-44865/.

[73] D. Kucevic, B. Tepe, S. Englberger, A. Parlikar, M. Mühlbauer, O. Bohlen, A. Jossen, H. Hesse, Standard battery energy storage system profiles: Analysis of various applications for stationary energy storage systems using a holistic simulation framework, J. Energy Storage 28 (2020) 101077, http://dx.doi.org/10.1016/j.est.2019.101077.

[74] S. Englberger, H. Hesse, N. Hanselmann, A. Jossen, SimSES multi-use: A simulation tool for multiple storage system applications, in: 2019 16th International Conference on the European Energy Market, EEM, 2019, pp. 1–5, http://dx.doi.org/10.1109/EEM.2019.8916568, URL https://ieeexplore.ieee.org/abstract/document/8916568/.

[75] L. Gerlach, T. Bocklisch, Experts versus algorithms? Optimized fuzzy logic energy management of autonomous PV hybrid systems with battery and H2 storage, Energies 14 (6) (2021) 1777, http://dx.doi.org/10.3390/en14061777.

[76] L. Desportes, I. Fijalkow, P. Andry, Deep reinforcement learning for hybrid energy storage systems: Balancing lead and hydrogen storage, Energies 14 (15) (2021) 4706, http://dx.doi.org/10.3390/en14154706.

[77] 50Hertz Transmission GmbH, Archive of mains frequency of ENTSO-e, 2021, URL https://www.50hertz.com/de/Transparenz/Kennzahlen/Regelenergie/ArchivNetzfrequenz.

[78] A. Parlikar, H. Hesse, A. Jossen, Topology and efficiency analysis of utility-scale battery energy storage systems, Atlantis Highlights Eng. 4 (2019) 119–131, http://dx.doi.org/10.2991/ires-19.2019.15.

[79] C. Weng, J. Sun, H. Peng, A unified open-circuit-voltage model of lithium-ion batteries for state-of-charge estimation and state-of-health monitoring, J. Power Sources 258 (2014) 228–237, http://dx.doi.org/10.1016/j.jpowsour.2014.02.026.

[80] Akkuplus.de, Panasonic - UR18650e - 3,7 volt 2150mah Li-Ion - EOL, 2020, URL https://akkuplus.de/Panasonic-UR18650E-37-Volt-2150mAh-Li-Ion-EOL.

[81] N. Damay, C. Forgez, M.-P. Bichat, G. Friedrich, Thermal modeling of large prismatic LiFePO 4 /graphite battery. Coupled thermal and heat generation models for characterization and simulation, J. Power Sources 283 (2015) 37–45, http://dx.doi.org/10.1016/j.jpowsour.2015.02.091.

[82] C. Forgez, D. Vinh Do, G. Friedrich, M. Morcrette, C. Delacourt, Thermal modeling of a cylindrical LiFePO4/graphite lithium-ion battery, J. Power Sources 195 (9) (2010) 2961–2968, http://dx.doi.org/10.1016/j.jpowsour.2009.10.105.

[83] B. Lei, W. Zhao, C. Ziebert, N. Uhlmann, M. Rohde, H. Seifert, Experimental analysis of thermal runaway in 18650 cylindrical li-ion cells using an accelerating rate calorimeter, Batteries 3 (4) (2017) 14, http://dx.doi.org/10.3390/batteries3020014.

[84] M.S. Rad, D.L. Danilov, M. Baghalha, M. Kazemeini, P.H.L. Notten, Thermal modeling of cylindrical LiFePO4 batteries, J. Mod. Phys. 04 (07) (2013) 1–7, http://dx.doi.org/10.4236/jmp.2013.47A2001.

[85] L.H. Saw, K. Somasundaram, Y. Ye, A. Tay, Electro-thermal analysis of lithium iron phosphate battery for electric vehicles, J. Power Sources 249 (2014) 231–238, http://dx.doi.org/10.1016/j.jpowsour.2013.10.052.

[86] A. Lidbeck, K.R. Syed, Experimental Characterization of Li-ion Battery cells for Thermal Management in Heavy Duty Hybrid Applications, (Ph.D. thesis), Department of Energy and Environment - Division of Electric Power Engineering, Chalmers University of Technology, 2017, URL http://publications.lib.chalmers.se/records/fulltext/252994/252994.pdf.

[87] K.K. Parsons, Design and Simulation of Passive Thermal Management System for Lithium-Ion Battery Packs on an Unmanned Ground Vehicle, (Ph.D. thesis), Faculty of California Polytechnic State University, 2012, URL https://digitalcommons.calpoly.edu/cgi/viewcontent.cgi?article=1961&context=theses.

[88] M.W. Tahir, Thermal characterization, multi-scale thermal modeling and experimental validation of lithium-ion batteries for automobile application, (Ph.D. thesis), University of Stuttgart, 2016, http://dx.doi.org/10.18419/OPUS-8775.

[89] A. Greco, Numerical and Analytical Modelling of Battery Thermal Management using Passive Cooling Systems, (Ph.D. thesis), Faculty of Science and Technology, Lancaster University, 2015, URL https://eprints.lancs.ac.uk/id/eprint/78600/1/2016AngeloGrecophd.pdf.

[90] akkuteile.de, Panasonic NCR18650 3,6v 2900mah (flat top) ungeschützt, 2020, URL https://www.akkuteile.de/lithium-ionen-akkus/18650/panasonic/panasonic-ncr18650_100605_1206.

[91] E-One Moli Energy, Molicel IHR18650c, 2020, URL https://www.custompower.com/documents/MOLICELIHR18650CDataSheetV1.0LC.pdf.

[92] A. Awarke, M. Jaeger, O. Oezdemir, S. Pischinger, Thermal analysis of a li-ion battery module under realistic EV operating conditions, Int. J. Energy Res. 37 (6) (2013) 617–630, http://dx.doi.org/10.1002/er.2884.

[93] A. Hales, L.B. Diaz, M.W. Marzook, Y. Zhao, Y. Patel, G. Offer, The cell cooling coefficient: A standard to define heat rejection from lithium-ion batteries, J. Electrochem. Soc. 166 (12) (2019) A2383–A2395, http://dx.doi.org/10.1149/2.0191912jes.

[94] P.E. Roth, Thermal Abuse Performance of MOLI, Panasonic and Sanyo 18650 Li-Ion Cells, Sandia National Laboratories, https://prod-ng.sandia.gov/techlib-noauth/access-control.cgi/2004/046721.pdf.

[95] Akkuplus.de, Sony - US26650FTC1 - 3,2 Volt 3000mah LiFePO4, 2020, URL https://akkuplus.de/Sony-US26650FTC1-32-Volt-3000mAh-LiFePO4.

[96] I. Tsiropoulos, D. Tarvydas., N. Lebedeva, Li-ion batteries for mobility and stationary storage applications - Scenarios for costs and market growth, JRC Science for Policy Report, 2018, http://dx.doi.org/10.2760/87175.

[97] C. Minke, T. Turek, Materials, system designs and modelling approaches in techno-economic assessment of all-vanadium redox flow batteries – A review, J. Power Sources 376 (2018) 66–81, http://dx.doi.org/10.1016/j.jpowsour.2017.11.058.

[98] J. Figgener, P. Stenzel, K.-P. Kairies, J. Linßen, D. Haberschusz, O. Wessels, M. Robinius, D. Stolten, D.U. Sauer, The development of stationary battery storage systems in Germany – status 2020, J. Energy Storage 33 (2021) 101982, http://dx.doi.org/10.1016/j.est.2020.101982.

[99] K. Mongird, V. Viswanathan, J. Alam, C. Vartanian, V. Sprenkle, Energy Storage Grand Challenge Cost and Performance Assessment 2020, U.S. Department of Energy / Pacific Northwest National Laboratory, 2020, DOE/PA-0204, URL https://www.pnnl.gov/sites/default/files/media/file/Final20-20ESGC20Cost20Performance20Report2012-11-2020.pdf.